A Computational Fluid Dynamics Design of a Carbon Dioxide Sorption Circulating Fluidized Bed

Benjapon Chalermsinsuwan and Pornpote Piumsomboon
Dept. of Chemical Technology, Fuels Research Center, Faculty of Science, Chulalongkorn University, Bangkok 10330, Thailand

Dimitri Gidaspow
Dept. of Chemical and Biological Engineering, Illinois Institute of Technology, Chicago, IL 60616

DOI 10.1002/aic.12213
Published online March 26, 2010 in Wiley Online Library (wileyonlinelibrary.com).

A kinetic theory based hydrodynamic model with experimentally determined sorption rates for reaction of CO_2 with K_2CO_3 solid sorbent is used to design a compact circulating fluidized bed sorption-regeneration system for CO_2 removal from flue gases. Because of high solids fluxes, the sorber does not require internal or external cooling. The output is verified by computing the granular temperatures, particle viscosities, dispersion, and mass transfer coefficients. These properties agree with reported measurement values except the radial dispersion coefficients, which are much higher due to the larger bed diameter. With the solid sorbent prepared according to published information, the CO_2 removal percentage at the riser top is 69.16%. To improve the CO_2 removal, an effort is needed to develop a better sorbent or to simply lower the inlet gas velocity to operate in a denser mode, leading to a larger system. Also, the effect of temperature rise on the removal efficiency is investigated. © 2010 American Institute of Chemical Engineers *AIChE J,* 56: 2805–2824, 2010

Keywords: circulating fluidized bed, computational fluid dynamics, sorption, kinetic theory, design

Introduction

Coal-fired utility boilers generate over 50% of the electricity in the United States. Energy Information Agency (EIA) of Department of Energy (DOE) projects that more than 300 GW of coal-fired electricity generating capacity currently in operation will be increased to nearly 450 GW by 2030.[1] Therefore, for the foreseeable future, coal will continue to play an important role in electricity generation, especially for base load power plants.

Emission of greenhouse gases such as carbon dioxide (CO_2) has increased over the past century. It is widely acknowledged that CO_2 emissions make the major contribution to global warming and their reduction is urgently needed.[2–4] To date, the capture of CO_2 emitted from major industries, such as the steel industry and power industry, has been proposed by many governments and major energy agencies. In 2007, traders bought and sold about 60 billion dollars worth of emissions allowances, mostly in Europe and Japan, where government regulate greenhouse gases. If, as expected, regulation comes to the United States, the market is expected to be worth 1 trillion dollars annually by the year 2020.[5]

Coal-fired power plants have made significant progress in reducing emissions of sulfur dioxide (SO_2), nitrogen oxide,

Correspondence concerning this article should be addressed to D. Gidaspow at gidaspow@iit.edu.

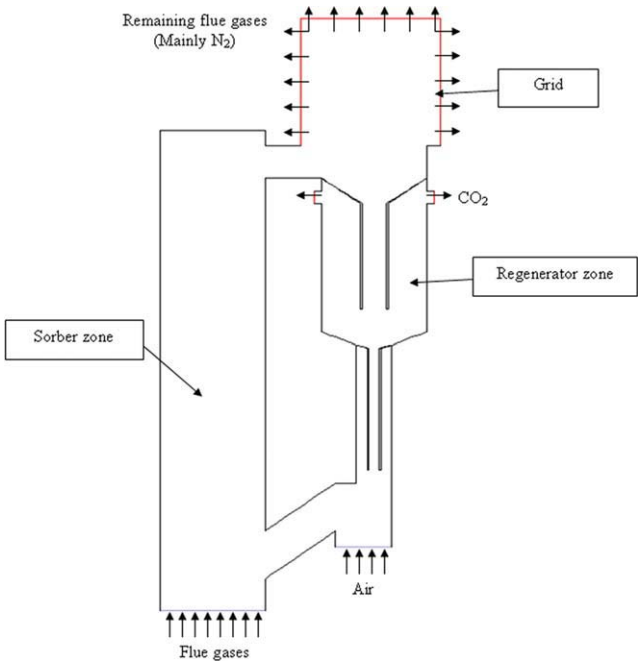

Figure 1. Novel compact sorption-regeneration circulating fluidized bed system.

[Color figure can be viewed in the online issue, which is available at wileyonlinelibrary.com.]

particulate matter, and mercury. At present, another challenge has arrived, the reduction of CO_2 emission. There are three main approaches for capturing the CO_2 generated from a primary fossil fuel, biomass, or mixtures of these fuels.[6]

Postcombustion systems separate CO_2 from flue gases produced by the combustion of the primary fuel in air. The concentration of CO_2 present in flue gas stream is typically 3–15% by volume, in which the main constituent is nitrogen from air. To capture these small fractions of CO_2, the systems normally use solid or liquid sorbents which are easy to integrate into the existing power plants. However, the energy requirement is still a problem for these systems. Chakma[7] calculated that over eighty percent of the total energy required for these systems is consumed in the regeneration step. To make the technology feasible on a reasonable scale, the alternatives utilizing less energy are needed.

Precombustion systems process the primary fuel in a reactor with steam and air or oxygen to produce a mixture consisting mainly of carbon monoxide and hydrogen. Additional hydrogen, together with CO_2, is produced by reacting the carbon monoxide with steam in a second shift reactor. The resulting mixture of hydrogen and CO_2 can then be separated into a CO_2 gas stream and a stream of hydrogen. If the CO_2 is stored, the hydrogen is a carbon-free energy carrier that can be combusted to generate power or heat. These systems are more elaborate than the postcombustion systems. They are suitable for CO_2 concentration of 15 to 60% by volume.

Oxyfuel combustion systems use oxygen instead of air for combustion of the primary fuel to produce a flue gas that is mainly water vapor and CO_2. The result is a flue gas with high CO_2 concentration which is greater than 80% by volume. The water vapor is then removed by cooling and compressing the gas stream. However, oxyfuel combustion requires the upstream separation of oxygen from air, with high purity. Further treatment of the flue gas may be needed to remove air pollutants and noncondensed gases.

For coal-fired power plants, the CO_2 concentration is $\sim$15% by volume or mole. Hence, a simple capture system using solid sorbents is suitable for this application. The solid sorbents capture CO_2 from flue gases through chemical absorption, physical adsorption, or a combination of the two effects. The objective of this study is to demonstrate how to use the recently developed kinetic theory based multiphase computational fluid dynamics (CFD) to design a system for capturing CO_2 in flue gases from coal fired power plant using solid sorbents. This is a major process system challenge because similar systems for sulfur removal were successfully designed but applied for a much smaller sulfur load.[8] Also, the systems should solve three main technical challenges which are the handling of large volumetric flow rate of the flue gases, the required power, and the quantity of CO_2 sorption.

Process system and solid sorbent descriptions

The novel compact sorption-regeneration circulating fluidized bed (CFB) is shown in Figure 1. The CFB system is selected because it can handle large volumetric flow rate of flue gases, which is one of the key technical challenges. This novel system consists of the sorption and regeneration in the same unit. The flue gases are fed at the bottom of the riser section which is designed to be a sorption zone. In this section, CO_2 and steam in the flue gases are absorbed into the solid sorbents. The remaining gases leave the system through the grid at the top of the downcomer section. The absorbed solid sorbents are regenerated in the downcomer section. Exhaust CO_2 and steam, which can be easily separated by conventional cooling process, leave the system via the outlet port at the top of the regeneration or desorption zone. Then, fresh solid sorbents are sent back to the riser section and again continue the sorption-regeneration cycle. At the bottom of the downcomer section, small amount of air at minimum fluidization velocity is fed to assist the circulation of solid sorbents.

Concerning the chemical reactions inside the system, Figures 2a, b show the block diagrams of sorption reaction with sorption temperature, T_S, and regeneration reaction with regeneration temperature, T_R, respectively. The sorption or absorption reaction is an exothermic reaction. Therefore there is heat release from the system. Applying the heat pump concept,[9,10] this lower temperature heat output can be transformed to a higher temperature heat input or required power for endothermic regeneration reaction, which is the second technical challenge for this system. To exchange the heat, the reactor may have the medium fluid flowing in a jacket at the wall. However, this is not the final configuration, the extension studies on energy requirement topic are still needed.

Regarding the last technical challenge about the absorbed CO_2 concentration, it can also be overcome if the solid sorbent is properly selected. The use of solid sorbents containing alkali and alkali-earth metals for CO_2 capture has been

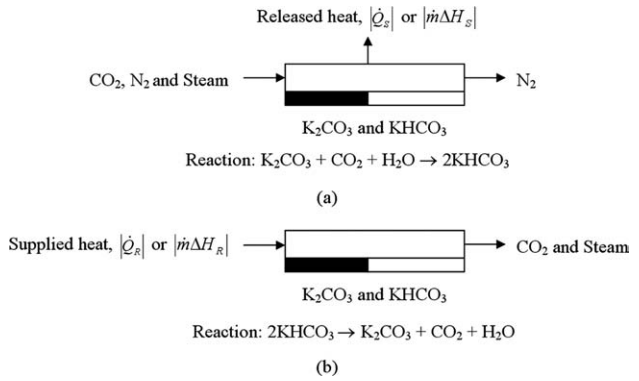

Figure 2. Block diagrams of (a) sorption or absorption reaction and (b) regeneration or desorption reaction.

reported in many articles.[11–13] In the proposed system, alkali based sorbents are considered because of their reactivity. Potassium carbonate (K_2CO_3) is chosen as the solid sorbent because its decomposition pressure is low, its CO_2 absorption capacity is high, and its heat of regenerative reaction is low near the room temperature.[14,15] Table 1 summarizes the heat of regenerative reaction for various preparations of alkaline carbonates. The overall K_2CO_3 solid sorbent reaction is

$$K_2CO_3 + CO_2 + H_2O \leftrightarrow 2KHCO_3 \quad (1)$$

Based on this stoichiometry, the theoretical or maximum weight percent of CO_2 on the solid sorbent can be up to 0.22. Hayashi et al.[16] also stated that K_2CO_3 solid sorbent reveals excellent properties for the capture of CO_2 when compared to other alkaline carbonates. Although the heat of regenerative reaction for lithium carbonate (Li_2CO_3) and sodium carbonate (Na_2CO_3) are lower than K_2CO_3, the decomposition pressure or the pressure reading coinciding with the first indication of decomposition of those solid sorbents appear to be too high, while the salts of rubidium (Rb_2CO_3) or cesium (Cs_2CO_3) require higher regeneration temperatures and they are expensive.

Computational fluid dynamics simulation

Hydrodynamics Model. In this study, a set of governing equations, mass, momentum, energy and species conservation equations, and constitutive equations were solved numerically. The constitutive equations are based on the kinetic theory of granular flow, as reviewed by Gidaspow.[17] This theory has been used by many researchers.[18–20] The commercial CFD program FLUENT 6.2.16 was chosen for modeling the system. There are several numerical models for gas–solid two-phase flow in the program such as, the Lagrangian model and the Eulerian model. The Lagrangian model should be used when the dispersed phase in the system occupies a low volume fraction and the Eulerian model should be used when the volume fraction of dispersed phase or solid sorbent cannot be occupied by the gas phase. In this case, the Eulerian model was selected. This approach solves the governing equations for each phase separately. A summary of the governing equations and constitutive equations is given in Table 2.

Chemical Reaction Model. The data needed for modeling the chemical reaction is the reaction rate equation. However, there is a lack of information given on reaction rate equation in the literature. Most of the researches focused only on the preparation and sorption characteristic of the sorbents. Onischak and Gidaspow[21] studied the feasibility of transferring CO_2 from the anode of a molten carbonate fuel cell to its cathode using solid K_2CO_3. They determined the rates of reaction in a parallel plate reactor as a function of time and CO_2 concentration in the range of 0.50 to 20.00% CO_2 and developed a reaction model. Onischak and Baker[22] made a sheet of the K_2CO_3 to be used for purifying air in portable life support systems for space travel. Later on, related studies at IIT using scanning electron microscopes by Ghezelayagh and Gidaspow[23] showed that in such sheets the small sorbent particles are held in a net of TEFLON fibers. As the reaction proceeds the sorbent particles undergo a structural change, as described in the model of Gidaspow.[14] Although past research deals with the preparation of sorbent sheets for stationary sorbers, it should be possible to use a similar preparation method for making spherical pellets for use in fluidized beds. Hirano et al.[24] proposed a modified chemical absorption method with a capability of cyclic fixed bed operations for the recovery of CO_2 from flue gases over K_2CO_3 solid sorbent. After their research, several studies regarding an efficient chemical absorption over K_2CO_3 solid sorbent, which was supported either on activated carbon or on other porous matrices such as silica (SiO_2), alumina (Al_2O_3), and vermiculite, were also reported using cyclic fixed bed operations under dry and moist conditions.[25,26] Sharanov et al.[27] proposed the kinetics of CO_2 sorption by a composite K_2CO_3 sorbent on Al_2O_3 support. The order of their sorption rate was found to be first order with respect to the CO_2 concentration. Recently, Park et al.[28] measured the breakthrough data of CO_2 to obtain the kinetics of the CO_2—K_2CO_3 reaction and showed that the concentration of water vapor in the feed stream affects the sorption rate of the CO_2 removal.

In order to simulate the novel sorption-regeneration CFB system, this study used the absorption reaction rate equation obtained by Gidaspow[14] and Onischak and Gidaspow.[21] Only the absorption reaction is considered due to the lack of chemical reaction data for regeneration of K_2CO_3 solid sorbent. In their studies, they stated that the sorption reaction rate is not affected greatly by water vapor content or humidity as long as sufficient water vapor is present to satisfy the

Table 1. The Heat of Regenerative Reaction for Various Preparations of Alkaline Carbonates

Compound	Heat of Regenerative Reaction at 298 K (MJ/kgmol)
Li_2CO_3	48.61
Na_2CO_3	129.16
K_2CO_3	137.41
Rb_2CO_3	148.84
Cs_2CO_3	157.21

Regeneration reaction for group 1A metal alkaline carbonates (M = metal of an alkaline):

$$2MHCO_3 \rightarrow M_2CO_3 + CO_2 + H_2O$$

Table 2. A Summary of the Governing Equations and Constitutive Equations

A. Governing Equations

(a) Conservation of mass;

– Gas phase;

$$\frac{\partial}{\partial t}\left(\varepsilon_g \rho_g\right) + \nabla \cdot \left(\varepsilon_g \rho_g v_g\right) = 0 \tag{2}$$

– Solid phase;

$$\frac{\partial}{\partial t}\left(\varepsilon_s \rho_s\right) + \nabla \cdot \left(\varepsilon_s \rho_s v_s\right) = 0 \tag{3}$$

(b) Conservation of momentum;

– Gas phase;

$$\frac{\partial}{\partial t}\left(\varepsilon_g \rho_g v_g\right) + \nabla \cdot \left(\varepsilon_g \rho_g v_g v_g\right) = -\varepsilon_g \nabla P + \nabla \cdot \tau_g + \varepsilon_g \rho_g g - \beta_{gs}\left(v_g - v_s\right) \tag{4}$$

– Solid phase;

$$\frac{\partial}{\partial t}\left(\varepsilon_s \rho_s v_s\right) + \nabla \cdot \left(\varepsilon_s \rho_s v_s v_s\right) = -\varepsilon_s \nabla P + \nabla \cdot \tau_s - \nabla P_s + \varepsilon_s \rho_s g + \beta_{gs}\left(v_g - v_s\right) \tag{5}$$

(c) Conservation of energy;

– Gas phase;

$$\frac{\partial}{\partial t}\left(\varepsilon_g \rho_g H_g\right) + \nabla \cdot \left(\varepsilon_g \rho_g v_g H_g\right) = -\varepsilon_g \frac{\partial P}{\partial t} + \tau_g : \nabla \cdot v_g + S_g + Q_{sg}, \tag{6}$$

with

$$H_g = \int c_{p,g} dT_g$$

– Solid phase;

$$\frac{\partial}{\partial t}\left(\varepsilon_s \rho_s H_s\right) + \nabla \cdot \left(\varepsilon_s \rho_s v_s H_s\right) = -\varepsilon_s \frac{\partial p_s}{\partial t} + \tau_s : \nabla \cdot v_s + S_s + Q_{gs}, \tag{7}$$

with

$$H_s = \int c_{p,s} dT_s$$

(d) Conservation of species;

– Gas phase;

$$\frac{\partial}{\partial t}\left(\varepsilon_g \rho_g y_j\right) + \nabla \cdot \left(\varepsilon_g \rho_g v_g y_j\right) = R_j \tag{8}$$

– Solid phase;

$$\frac{\partial}{\partial t}\left(\varepsilon_s \rho_s y_j\right) + \nabla \cdot \left(\varepsilon_s \rho_s v_s y_j\right) = R_j \tag{9}$$

(e) Conservation of solid phase fluctuating energy;

$$\frac{3}{2}\left[\frac{\partial}{\partial t}\left(\varepsilon_s \rho_s \theta\right) + \nabla \cdot \left(\varepsilon_s \rho_s \theta\right) v_s\right] = \left(-\nabla p_s \mathrm{I} + \tau_s\right) : \nabla v_s + \nabla \cdot \left(\kappa_s \nabla \theta\right) - \gamma_s \tag{10}$$

Table 2. (Continued)

B. Constitutive Equations;

(a) Gas phase stress;

$$\tau_g = \varepsilon_g \mu_g \left[\nabla v_g + \left(\nabla v_g\right)^T\right] - \frac{2}{3}\varepsilon_g \mu_g \left(\nabla \cdot v_g\right) I \tag{11}$$

(b) Solid phase stress;

$$\tau_s = \varepsilon_s \mu_s \left[\nabla v_s + \left(\nabla v_s\right)^T\right] - \varepsilon_s \left(\xi_s - \frac{2}{3}\mu_s\right) \nabla \cdot v_s I \tag{12}$$

(c) Collisional dissipation of solid fluctuating energy;

$$\gamma_s = 3\left(1 - e^2\right)\varepsilon_s^2 \rho_s g_0 \theta \left(\frac{4}{d_p}\sqrt{\frac{\theta}{\pi}}\right) \tag{13}$$

(d) Radial distribution function;

$$g_0 = \left[1 - \left(\frac{\varepsilon_s}{\varepsilon_{s,\max}}\right)^{1/3}\right]^{-1} \tag{14}$$

(e) Solid phase pressure;

$$p_s = \varepsilon_s \rho_s \theta \left[1 + 2 g_0 \varepsilon_s \left(1 + e\right)\right] \tag{15}$$

(f) Solid phase shear viscosity;

$$\mu_s = \frac{4}{5}\varepsilon_s \rho_s d_p g_0 \left(1+e\right)\sqrt{\frac{\theta}{\pi}} + \frac{10 \rho_s d_p \sqrt{\pi \theta}}{96\left(1+e\right) g_0 \varepsilon_s}\left[1 + \frac{4}{5} g_0 \varepsilon_s \left(1+e\right)\right]^2 \tag{16}$$

(g) Solid phase bulk viscosity;

$$\xi_s = \frac{4}{3}\varepsilon_s \rho_s d_p g_0 \left(1+e\right)\sqrt{\frac{\theta}{\pi}} \tag{17}$$

(h) Conductivity of the fluctuating energy;

$$\kappa_s = \frac{150 \rho_s d_p \sqrt{\theta \pi}}{384\left(1+e\right) g_0}\left[1 + \frac{6}{5}\varepsilon_s g_0 \left(1+e\right)\right]^2 + 2\rho_s \varepsilon_s^2 d_p \left(1+e\right) g_0 \sqrt{\frac{\theta}{\pi}} \tag{18}$$

(i) Gas-solid phase interphase exchange coefficient;

when $\varepsilon_g \leq 0.80$;

$$\beta_{gs} = 150\frac{\left(1-\varepsilon_g\right)^2 \mu_g}{\varepsilon_g d_p^2} + 1.75\frac{\left(1-\varepsilon_g\right)\rho_g \left|v_g - v_s\right|}{d_p}, \tag{19}$$

when $\varepsilon_g > 0.80$;

$$\beta_{gs} = \frac{3}{4}\frac{\left(1-\varepsilon_g\right)\varepsilon_g}{d_p}\rho_g \left|v_g - v_s\right| C_{D0} \varepsilon_g^{-2.65}, \tag{20}$$

With

$Re_k < 1000$; $C_{D0} = \frac{24}{Re_k}\left(1 + 0.15 Re_k^{0.687}\right)$; $Re_k = \frac{\rho_g \varepsilon_g \left|v_g - v_s\right| d_p}{\mu_g}$

$Re_k \geq 1000$; $C_{D0} = 0.44$

reaction stoichiometry which is consistent with the input condition in this study. This is different from the result of Park et al.[28] Therefore, they proposed an equation as a first order reaction with respects to CO_2 concentration (C_{CO_2}) and volume fraction of K_2CO_3 solid sorbent (ε_s). Their sorption reaction rate equation (r) is:

$$r = -k_{\text{reaction}} C_{CO_2} \varepsilon_s \tag{21}$$

where k_{reaction} = Reaction rate constant = 1.95 s^{-1}.

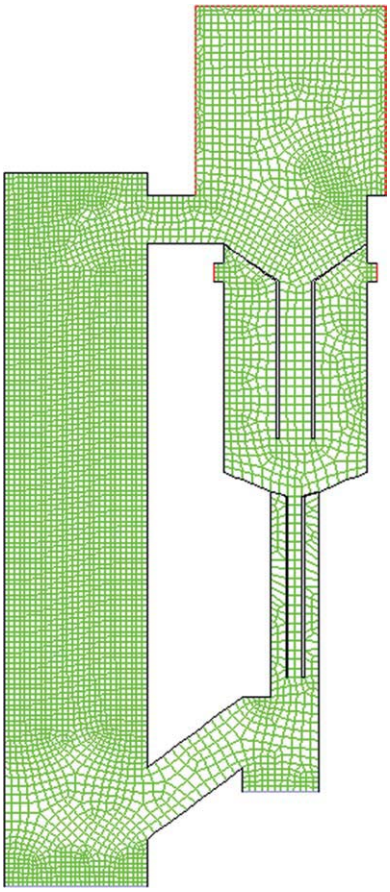

Figure 3. Computational domain of the novel circulating fluidized bed system.

[Color figure can be viewed in the online issue, which is available at wileyonlinelibrary.com.]

Since the heterogeneous reaction rate equation is not available in the FLUENT 6.2.16 program, the new additional UDF (user-defined function) code written in C programming language was added. To solve the regeneration reaction model, which at present is not available, we directly set the condition of recirculated solid sorbents from the downcomer section to the riser section as a fresh or new solid sorbents.

System and Computational Domain Description. The complete set of equations shown previously was used to obtain the hydrodynamics and chemical reaction in the novel sorption-regeneration CFB system as shown in Figure 1. This CFB system is a modified version of an actual PYROFLOW CFB system built for Goodrich in IL. This system had been used for simulating SO_2 sorption reaction.[8] The diameter (D) and height (h) of their riser section were 3.0 and 15.0 m, respectively, while the diameter (D) and height (h) of the downcomer section were 3.0 (at widest position) and 16.7 m, respectively. As a three dimensional model requires long computation time and as there is no specific experimental measurement for comparison, this study used a two dimensional model for the simulation.

The computational domain of the novel system is illustrated in Figure 3. It consists of 5500 computational cells. A time step of 0.001 s with 100 iterations per time step was used to ensure numerical stability. The models were solved by using a computer with Pentium 1.80 GHz CPU 2 GB RAM. It took ~10 days of computer time for 40 s of simulation time.

Initial and Boundary Conditions. This study mainly used the operating parameter from Therdthianwong and Gidaspow[8] simulation. At the inlet, the velocity, volume fraction, temperature, and gas species composition were specified, as summarized in Table 3. On the other hand, at the outlet, the system pressure was specified as atmospheric pressure. Initially, there were K_2CO_3 solid sorbents inside the system with a volume fraction of 0.50 and the height of K_2CO_3 solid sorbents in the riser and downcomer sections were 4.5 and 12.5 m, respectively. The temperature of K_2CO_3 solid sorbents were set as 343.15 K. At the wall, an adiabatic condition was used and a no slip condition was applied for all velocities, except for the tangential velocity of the solid phase and the granular temperature. Here, the boundary conditions of Johnson and Jackson[29] were used. These conditions were first applied in the kinetic theory of granular flow modeling by Sinclair and Jackson.[30] They are:

$$v_{st,W} = -\frac{6\mu_s \varepsilon_{s,max}}{\pi\phi\rho_s \varepsilon_s g_0 \sqrt{3\theta}} \frac{\partial v_{st,W}}{\partial n}, \tag{22}$$

$$\theta_W = -\frac{\kappa_s \theta}{\gamma_W} \frac{\partial \theta_W}{\partial n} + \frac{\sqrt{3}\pi\phi\rho_s \varepsilon_s v_{s,slip}^2 g_0 \theta^{\frac{3}{2}}}{6\varepsilon_{s,max}\gamma_W}, \tag{23}$$

where

$$\gamma_W = \frac{\sqrt{3}\pi(1-e_W^2)\varepsilon_s \rho_s g_0 \theta^{3/2}}{4\varepsilon_{s,max}}.$$

Results and Discussion

The results can be divided into two main parts: hydrodynamics and chemical reaction behavior. In the hydrodynamics part, the flow structure and system parameters inside the novel system are calculated and matched with the literature. Then the effect of hydrodynamics behavior on reaction characteristic is discussed in the chemical reaction behavior part. Also, the effect of temperature rise on the chemical reaction is discussed. The first step in the design of the CFB sorber is the computation of correct hydrodynamics. The computer code must calculate the system parameters that match the experimental data in the range of desired particle diameters and flow rates. The FLUENT and similar codes can easily compute system parameters that are orders of magnitude smaller or larger than the measured values.

Hydrodynamics behavior

K_2CO_3 Solid Sorbent Volume Fraction. Figure 4 displays the transient distributions of K_2CO_3 solid sorbent volume fraction inside the novel CFB system. The system is made up of the dilute region in the riser section and the dense region in the downcomer section. In the riser section a strong asymmetric volume fraction is computed because of the inlet–outlet configuration which usually found in the literature experiments.[31,32] At the top of the downcomer section, the K_2CO_3 solid sorbent accumulates at the grid and falls back into the regeneration zone. Because of the

Table 3. Parameters Used for the Simulation

Symbol	Description	Value
ρ_g	Gas density	1.206 kg/m^3
μ_g	Gas viscosity	2×10^{-5} kg/m s
ρ_s	Solid sorbent density	1530 kg/m^3
d_p	Solid sorbent diameter	210 μm
G_s	Solid sorbent circulation rate (for $v_g = 3$ m/s)	635 kg/m^2 s
e	Restitution coefficient between particles	0.90
e_W	Restitution coefficient between particle and wall	0.80
ϕ	Specularity coefficient	0.01
t	Simulation time	40 s
At the bottom of the riser section		
v_g	Inlet gas velocity	3 m/s (nonuniform profile)
ε_g	Inlet gas volume fraction	1.00
T_g	Inlet gas temperature	343.15 K
y_{CO_2}	Inlet CO_2 species mole fraction	0.15
y_{H_2O}	Inlet steam species mole fraction	0.15
y_{Air}	Inlet air species mole fraction	0.70
At the bottom of the downcomer section		
v_g	Inlet gas velocity	0.025 m/s (uniform profile)
ε_g	Inlet gas volume fraction	1.00
T_g	Inlet gas temperature	298.15 K
y_{CO_2}	Inlet CO_2 species mole fraction	0.00
y_{H_2O}	Inlet steam species mole fraction	0.00
y_{Air}	Inlet air species mole fraction	1.00

regeneration zone geometry, it induces high contacting or mixing of K_2CO_3 solid sorbent that will increase the reaction conversion.

Figure 5 depicts the time- and area-averaged K_2CO_3 solid sorbent volume fraction profiles in the riser section of the novel system with four different time-averaged ranges. The 0–40 s time-averaged result does not compare well with the other time-averaged ranges. The time-averaged results change only slightly after the simulation time of 5 s. This implies that the system has reached the quasi steady-state condition. In this study, the model with time averaging between 10 and 40 s was selected as a representative system. After the system reaches quasi steady state, the computed profile is of the desirable C type, except at the bottom section. This deviation is due to the inlet effect. The high volume fraction at the top of the riser is affected by the riser outlet type. This solid distribution profile is similar to the observed behavior in the large scale industrial CFB.[33,34] The K_2CO_3 solid sorbent volume fraction at the bottom and at the top of the riser are in the range of 0.18 to 0.28 and 0.13 to 0.14, respectively. Because of this variation of the K_2CO_3 solid sorbent volume fraction profiles the solid sorbents are not well distributed or mixed in the axial direction. This will make the chemical reaction or the rate of CO_2 removal to be nonhomogeneous throughout the riser system.

To illustrate asymmetric profiles, the time-averaged K_2CO_3 solid sorbent volume fraction distributions in the riser section at three locations; right wall, center, and left wall (wall opposite to the regenerated sorbent inlet) are plotted in Figure 6. The profiles show a denser region at the right wall and more dilute region at the left wall especially at the bottom section of the riser. The results are consistent with the radial distributions of time-averaged K_2CO_3 solid sorbent volume fraction at riser heights of 3.5, 7.5, and 11.5 m as shown in Figure 7. These three different heights are

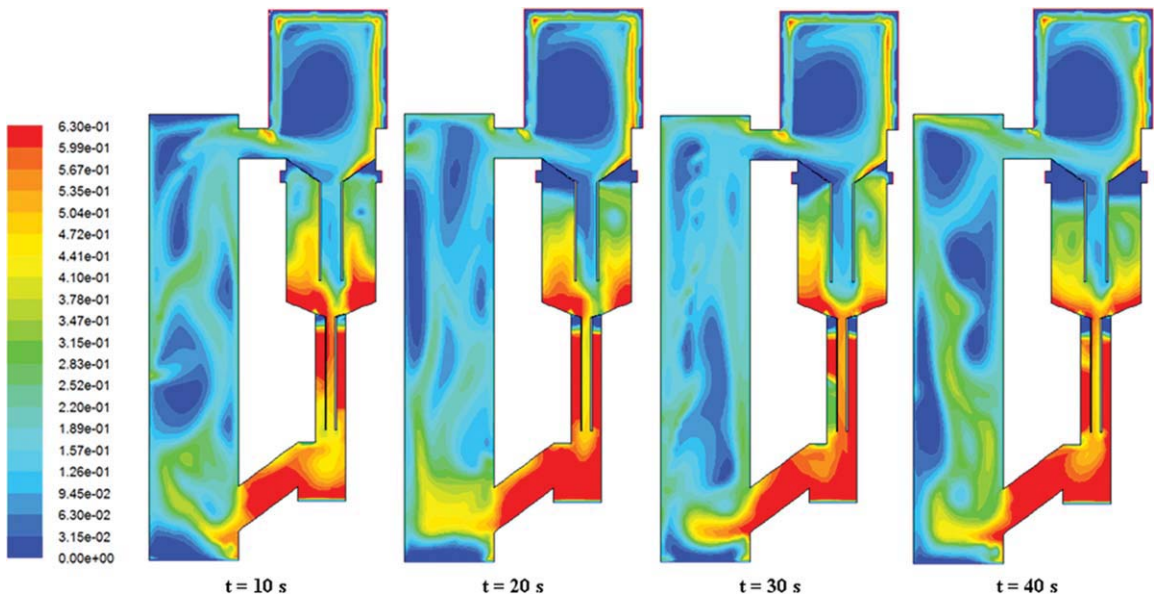

Figure 4. Transient distributions of K_2CO_3 solid sorbent volume fraction inside the novel circulating fluidized bed system.

[Color figure can be viewed in the online issue, which is available at wileyonlinelibrary.com.]

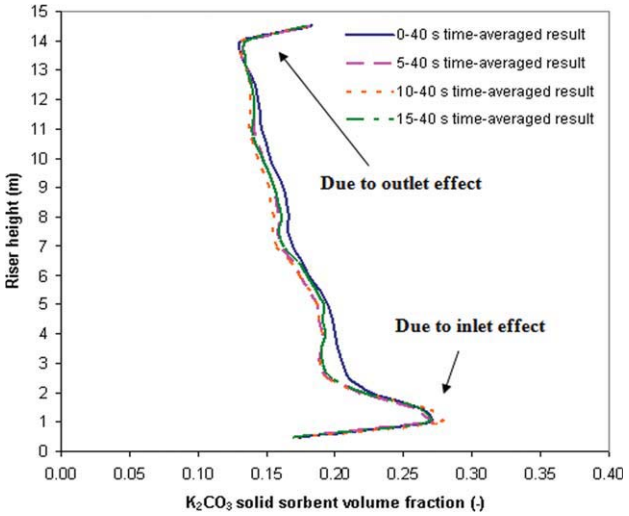

Figure 5. Time- and area-averaged K_2CO_3 solid sorbent volume fraction profiles in the riser section of the novel circulating fluidized bed system with four different time-averaged ranges.

[Color figure can be viewed in the online issue, which is available at wileyonlinelibrary.com.]

selected to represent the bottom, center, and top of the riser. Also, the numerical simulations predict the core-annular flow structure, similar to the experimentally observed flow pattern. In the core region of the riser (center), the profile is almost flat and more dilute than at the wall region. The K_2CO_3 solid sorbent volume fraction at the wall is higher because the solid sorbents are flowing downward. The downflow of K_2CO_3 solid sorbent is an indication of the back mixing inside the system which increases the opportunity for K_2CO_3 solid sorbent to react. However, this flow behavior

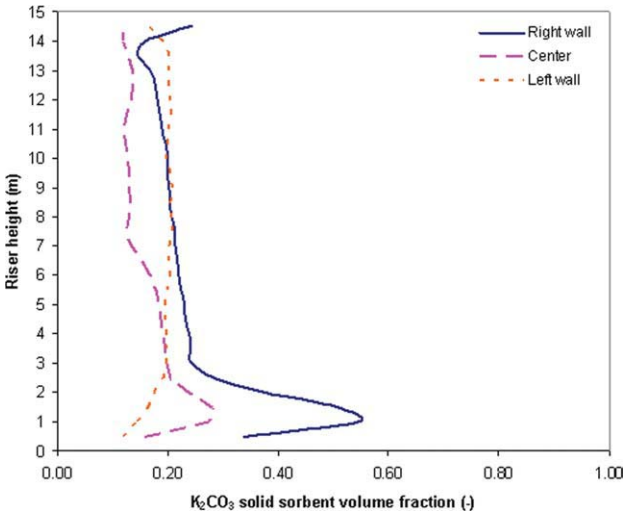

Figure 6. Time-averaged K_2CO_3 solid sorbent volume fraction distributions in the riser section at three locations.

[Color figure can be viewed in the online issue, which is available at wileyonlinelibrary.com.]

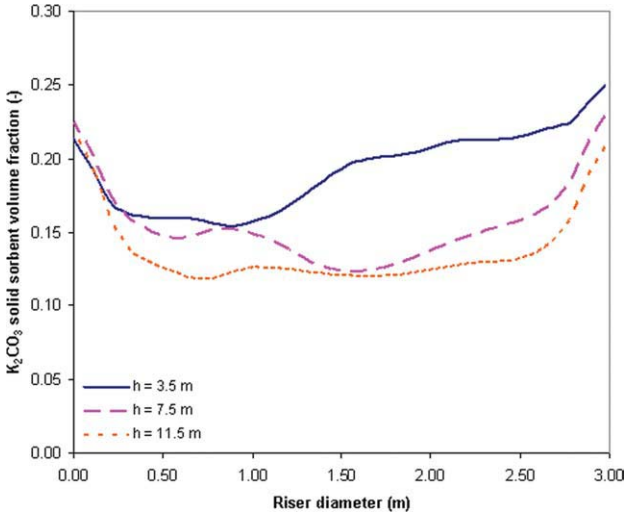

Figure 7. Radial distributions of time-averaged K_2CO_3 solid sorbent volume fraction at three different riser heights.

[Color figure can be viewed in the online issue, which is available at wileyonlinelibrary.com.]

also has a disadvantage because it will make the rate of CO_2 removal to be heterogeneous in the radial direction.

In addition, the system pressure drop relates to the K_2CO_3 solid sorbent volume fraction. The vertical pressure gradient is a direct measurement of the cross-sectional average solid volume fraction.[35,36] The system pressure drop profile decreases along the riser height owing to the decreasing of K_2CO_3 solid sorbents. Over this riser system, the K_2CO_3 solid sorbent leads to a system pressure drop of about 2467 Pa/m which is also comparable with the system pressure drop over the other industrial scale riser.[37]

No numerical modeling is complete without a study of mesh refinement study. Before moving to the next parts, the effect of computational cell on modeling result is investigated. The computational cell increases with the finer of the grid. To prove that the result is independent of the number of cells, a grid independence was performed. Ideally, the grid should be sufficiently fine so that further refinement does not change the result. Figure 8 shows the time- and area-averaged K_2CO_3 solid sorbent volume fraction profiles in the riser section of the novel system with three different grids or computational cells. The domains consist of 5500, 6875, and 8250 computational cells. All the computational cells predict similar solid sorbent volume fraction profiles. This indicates that all the grids are sufficiently fine for providing reliable results. In this study, the computational domain consisting of 5500 computational cells was chosen for further study.

K_2CO_3 Solid Sorbent and Gas Velocities. Figure 9 displays the transient distributions of K_2CO_3 solid sorbent axial velocity vector. The results match with the results from the previous figures and confirm the downward flow of K_2CO_3 solid sorbent at the top and near the wall of the riser section. In the downcomer section, a core-annular flow pattern of K_2CO_3 solid sorbent is observed in the regeneration zone which will provide more residence time for K_2CO_3 solid

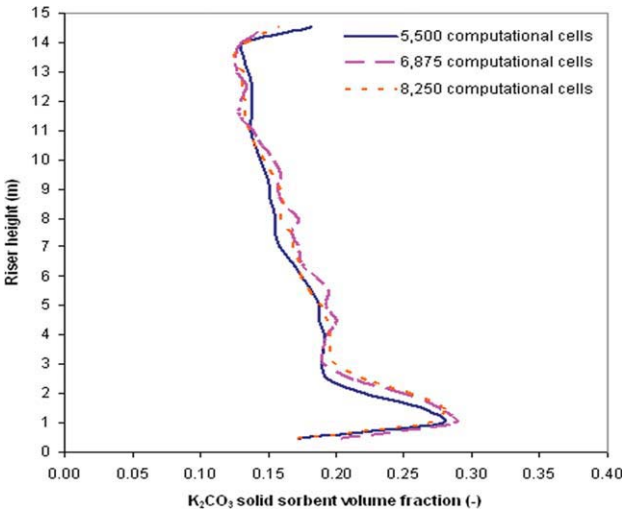

Figure 8. Time- and area-averaged K_2CO_3 solid sorbent volume fraction profiles in the riser section of the novel circulating fluidized bed system with three different grids or computational cells.

[Color figure can be viewed in the online issue, which is available at wileyonlinelibrary.com.]

sorbent to reside which will increase the conversion of the chemical reaction.

The radial distributions of the time-averaged axial velocity profile for K_2CO_3 solid sorbent and gas phases at various heights in the riser section are shown in Figure 10. Figure 11 illustrates the radial distributions of the time-averaged radial velocity profile for K_2CO_3 solid sorbent and gas phases at various heights in the riser section. All the velocity profiles of K_2CO_3 solid sorbent and gas have similar trends. However, there is a slip velocity between the two phases because of the density difference. The gas phase has higher velocity than the K_2CO_3 solid sorbent phase. At lower section in the riser, the axial velocity profiles are strongly asymmetric, consistent with the K_2CO_3 solid sorbent volume fraction profiles. A comparison between the velocity components shows that the axial velocity is much higher than the radial velocity in both phases. This is because the system flow is mainly in the axial direction.

K_2CO_3 Solid Sorbent Granular Temperature. Tartan and Gidaspow[32] used the kinetic theory based particle image method to determine the velocity oscillations; both due to individual particles called "laminar granular temperature" and due to particle clusters called "turbulent granular temperature". To compute the granular temperature, the related equations have to be programmed into the CFD codes. The code itself computes the laminar granular temperature. The turbulent granular temperature is defined as the average of the normal Reynolds stresses, which is the average of the three squares of the velocity fluctuation components ($\overline{v_i' v_i'}$) in the three directions. For two-dimensional simulation, the velocity fluctuations in the nonflow or radial directions, x- and z- directions, are assumed to be equal. The turbulent granular temperature (θ_t) can be calculated as follows:

$$\theta_t(t,x) \cong \frac{2}{3}\overline{v_x' v_x'} + \frac{1}{3}\overline{v_y' v_y'}. \tag{24}$$

The sum of the granular temperatures due to the particle oscillations and due to the particle cluster oscillations is the total granular temperature. Figure 12 compares the height-averaged total granular temperature from this study with those from literatures summarized by Kashyap et al.[38] The value of the total granular temperature of 4 m^2/s^2 is somewhat higher than the measured values, but it is reasonable in view of the high particle velocity of 6 m/s. The granular temperatures for these particles are primarily due to shear stress.

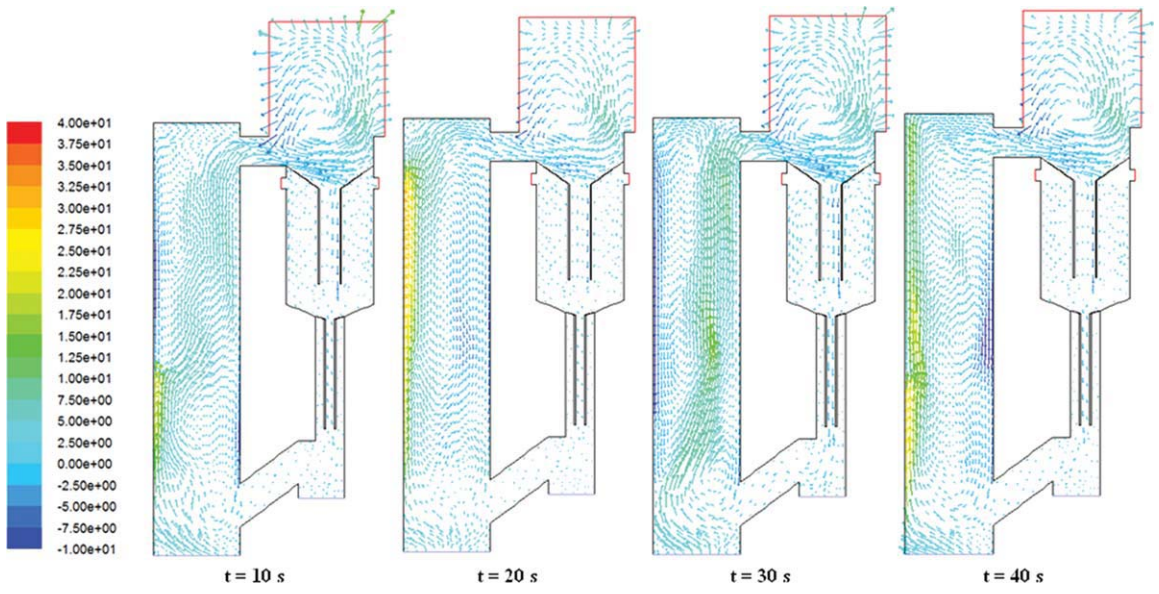

Figure 9. Transient distributions of K_2CO_3 solid sorbent axial velocity vector.

[Color figure can be viewed in the online issue, which is available at wileyonlinelibrary.com.]

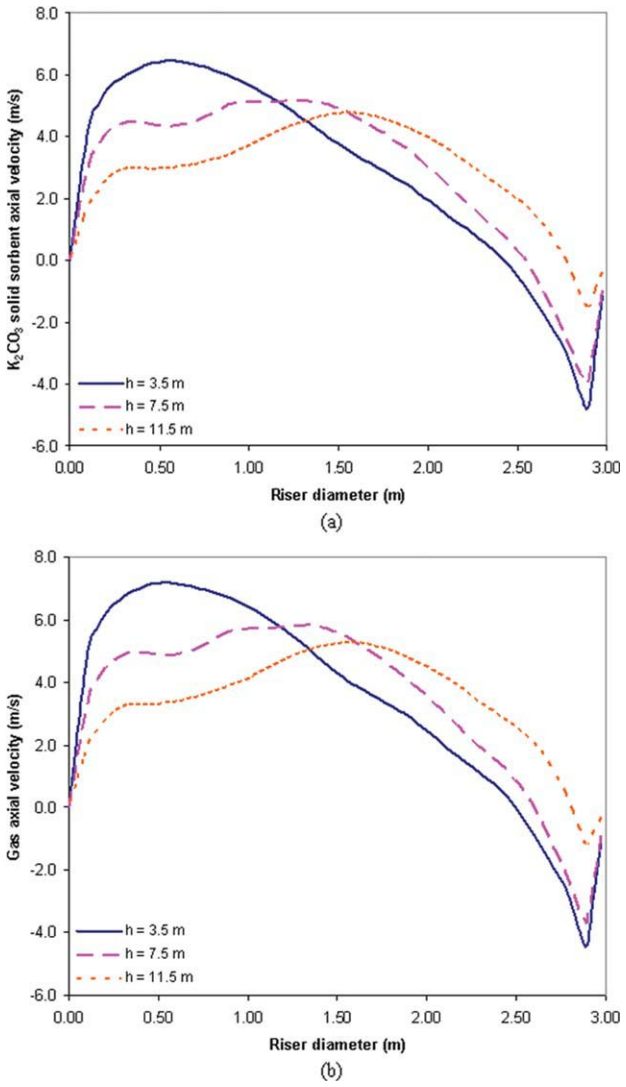

Figure 10. Radial distributions of the time-averaged axial velocity profile for (a) K_2CO_3 solid sorbent and (b) gas phases in the riser section at various heights.

[Color figure can be viewed in the online issue, which is available at wileyonlinelibrary.com.]

K_2CO_3 Solid Sorbent Viscosity. From the kinetic theory of granular flow, the solid viscosity is a function of granular temperature.[39] The total granular temperature, which is the overall system oscillation, is substituted in Eq. 16 to calculate the solid viscosity. Figure 13 displays computed solid viscosities as a function of solid volume fraction. The solid viscosity increases with the increasing solid volume fraction, consistent with the typical observation. In the figure, the trend from modified literature correlation for K_2CO_3 solid sorbent diameter is also shown with the new obtained correlation constant of 0.055. The proposed correlation is as follows;

$$\mu_s = 0.055\varepsilon_s^{1/3} g_0, \tag{25}$$

The high particle viscosities, up to one poise, are reasonable in view of the high granular temperatures.

K_2CO_3 Solid Sorbent and Gas Dispersion Coefficients. There are two kinds of mixing in fluidization: one due to individual particle oscillations and the other due to particle cluster oscillations or turbulence. An order of magnitude estimate of the dispersion coefficients due to individual particles oscillations can be obtained from the laminar granular temperature.[37,40] In this study, in order to compare solid and gas dispersion coefficients, we focus on the dispersion coefficient due to particle cluster oscillations or turbulence (D_i). It can be obtained as a function of normal Reynolds stress and the Lagrangian integral time scale (T_L) as expressed in Eq. 26. The subscript is "i" because the dispersion coefficient can be calculated in both the axial (y) and the radial (x) directions.

$$D_i(r) = \overline{v_i' v_i'(r)} T_L, \tag{26}$$

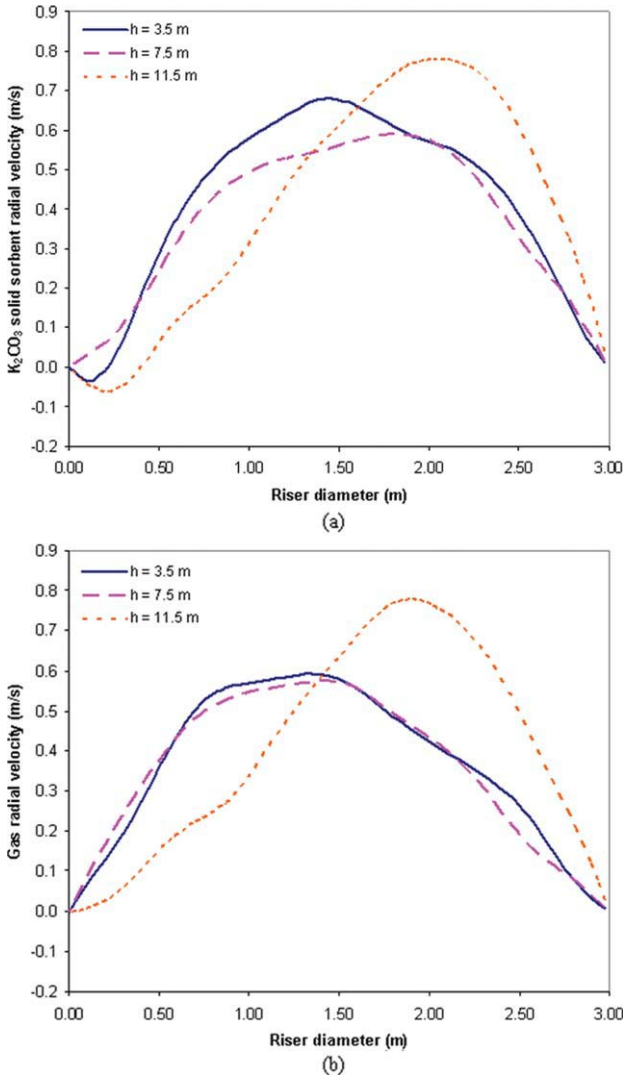

Figure 11. Radial distributions of the time-averaged radial velocity profile for (a) K_2CO_3 solid sorbent and (b) gas phases in the riser section at various heights.

[Color figure can be viewed in the online issue, which is available at wileyonlinelibrary.com.]

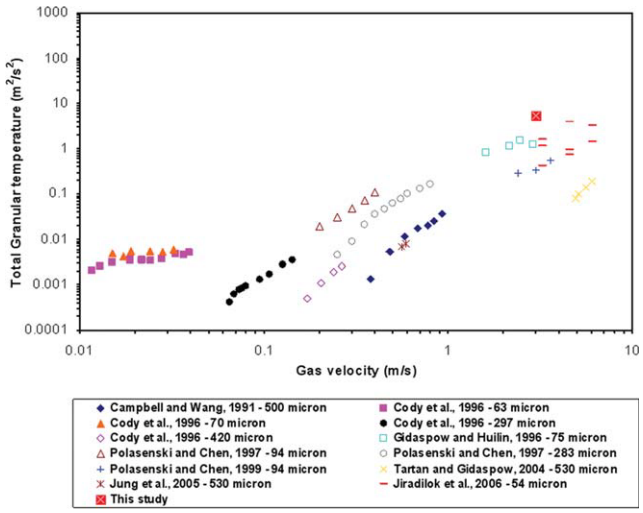

Figure 12. Comparison of total granular temperatures with the literature values.

[Color figure can be viewed in the online issue, which is available at wileyonlinelibrary.com.]

Where the Lagrangian integral time scale of the particle motion is defined by:

$$T_L = \int_0^\infty \frac{\overline{v'(t)v'(t+t')}}{\overline{v'^2}} dt', \tag{27}$$

A comparison of the radial and axial solid and gas dispersion coefficients at various heights in the riser section of the novel system is summarized in Table 4. Also, the averaged values are shown. All dispersion coefficients vary from top to bottom of the riser, as expected. Although the solid and gas dispersion coefficients are higher in the middle region of the riser, this phenomenon is not always the case. With other system conditions, the solid and gas dispersion coefficients are sometimes lower in the middle region. Here, the radial

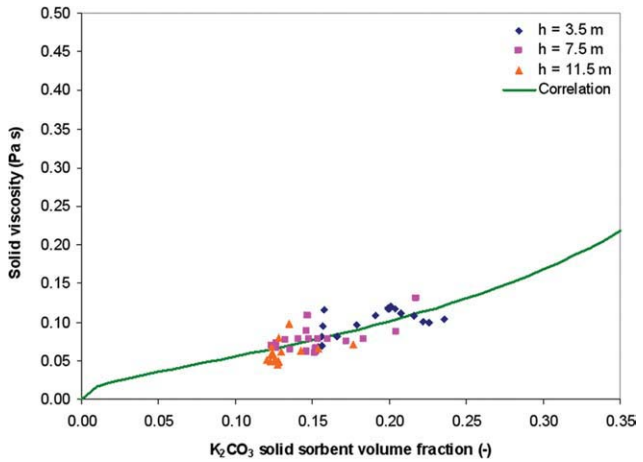

Figure 13. Comparison of solid viscosities with the modified literature correlation.

[Color figure can be viewed in the online issue, which is available at wileyonlinelibrary.com.]

Table 4. Computed Information on the Axial and Radial Dispersion Coefficients at Three Different Heights in the Riser Section of the Novel Circulating Fluidized Bed System

	Solid Dispersion Coefficients (m^2/s)		Gas Dispersion Coefficients (m^2/s)	
Riser Height (m)	Axial	Radial	Axial	Radial
3.5	0.2825	0.2231	0.3344	0.2280
7.5	0.7536	0.0105	0.7662	0.0107
11.5	0.2566	0.0300	0.2983	0.0304
Averaged	0.4309	0.0879	0.4663	0.0897

dispersion coefficients in the riser are one order of magnitude lower than the axial ones. The gas dispersion is higher than the solid dispersion because of the slip velocity between the phases.

The comparisons between the computed solid dispersion coefficients due to particle cluster oscillations for axial and radial directions and the literature surveyed by Chalermsinsuwan et al.[37] are shown in Figures 14. Figure 15 displays the comparisons of computed axial and radial gas dispersion coefficients with the same literature survey. The computations show that the axial, solid and gas, dispersion coefficients are in reasonable agreement with the measurements; while the radial, solid and gas, dispersion coefficients are higher than the measurements in a similar inlet gas velocity range. The explanation for the high radial, solid and gas, dispersion coefficients are that in this study an industrial scale riser system is considered. It has an extremely large diameter when compared to the laboratory scale riser system in the literature survey. Thus, the effect from the wall will have less impact on the solid and gas dispersions. The solid and gas in the large system have more opportunity to mix than in the small systems. Here, the radial solid dispersion coefficient of about 0.10 m^2/s is excellent. But it is still not high enough to eliminate the undesirable core-annular flow behavior.

Mass Transfer Coefficient and Sherwood Number. Chalermsinsuwan et al.[41] proposed two methodologies for computation of mass transfer coefficients and Sherwood numbers in fluidized beds. Their methodology for computation of mass transfer coefficient and Sherwood number from the concentration data is used. Integration of conservation of species equation over time and over the riser diameter for CO_2 species gives the one dimensional steady state balance. Substituting the rate of reaction and solving the equation gives:

$$\ln C_{CO_2} = \ln C_{CO_2,0} - \frac{K\varepsilon_s}{v_y \varepsilon_g} Y, \tag{28}$$

where K is the overall resistance, ε_g is the volume fraction of gas phase, v_y is the velocity of gas phase in axial or vertical direction, Y is the axial or vertical distance and the subscript "0" is the initial molar concentration of CO_2. To compare the results, the computations were focused on three different riser sections similar to the results in previous parts. In these sections, the computed, solid and gas, volume fractions and velocities are not considerably different.

The linear plot of natural logarithm of CO_2 molar concentration vs. the height of the riser gives the slope, which further gives the overall resistance. In the simulation, the

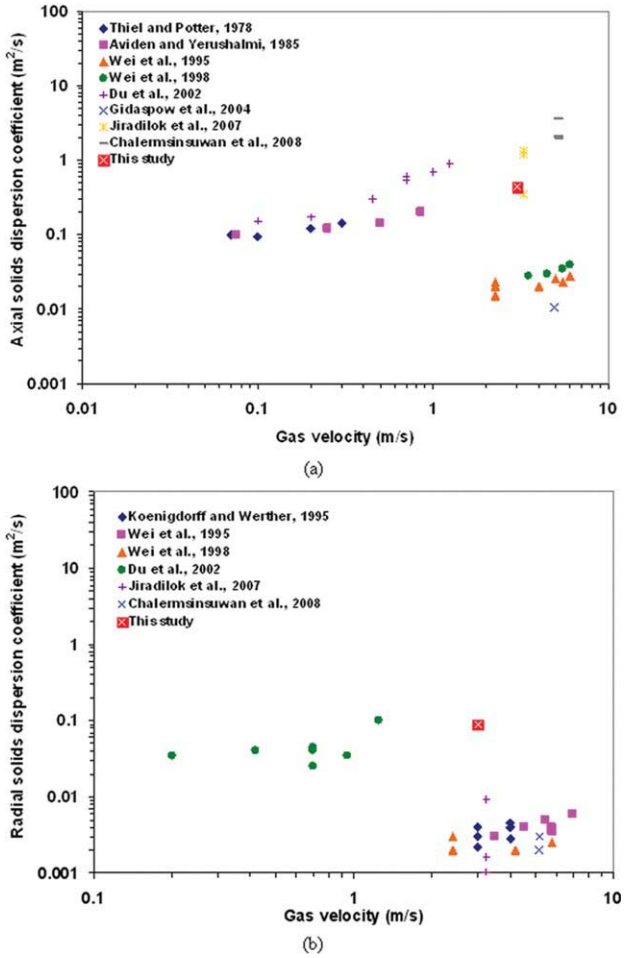

Figure 14. Effect of the gas velocity on (a) axial and (b) radial solid dispersion coefficients.

[Color figure can be viewed in the online issue, which is available at wileyonlinelibrary.com.]

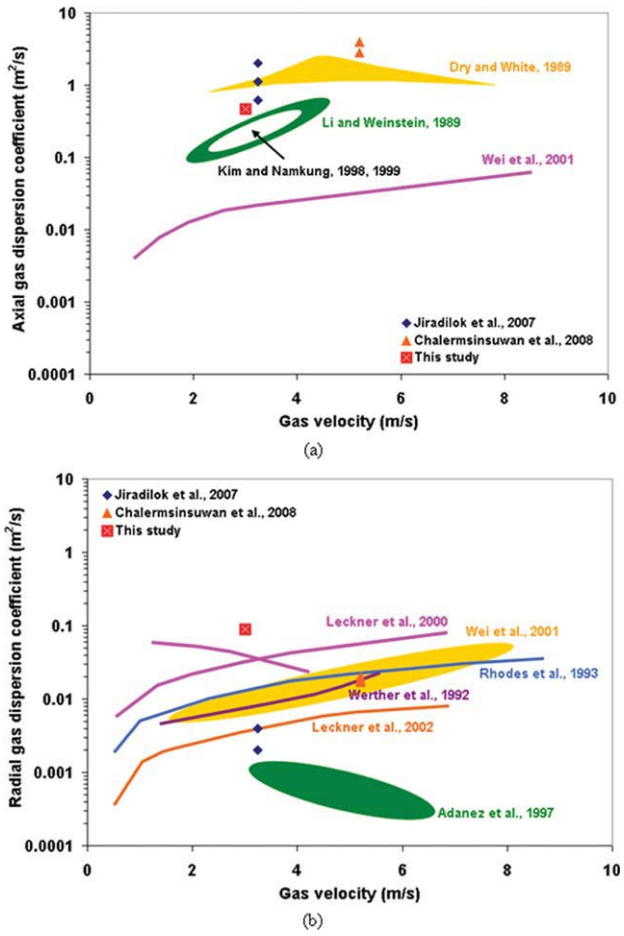

Figure 15. Effect of the gas velocity on (a) axial and (b) radial gas dispersion coefficients.

[Color figure can be viewed in the online issue, which is available at wileyonlinelibrary.com.]

reaction rate constant is an input. The conventional additive resistance concept, then, permits us to compute the mass transfer coefficient ($k_{\text{mass transfer}}$) as follows:

$$\frac{1}{K} = \frac{1}{k_{\text{mass transfer}} a_v} + \frac{1}{k_{\text{reaction}}}, \tag{29}$$

where a_v is the external surface per volume of solid sorbent.

The Sherwood number (Sh) is then given by Eq. 30 below:

$$Sh = \frac{k_{\text{mass transfer}} d_p}{D}, \tag{30}$$

where D is molecular diffusivity.

Table 5 summarizes the computed information on mass transfer coefficients and Sherwood numbers at three different heights in the riser section of the novel system. The computed mass transfer coefficients and Sherwood numbers decrease with the riser height and reach small values at the top section. This variation of the Sherwood numbers is similar to the typical behavior in convective mass transport. The fact that the overall resistance and the reaction rate constant

Table 5. Computed Information on the Mass Transfer Coefficients and Sherwood Numbers at Three Different Heights in the Riser Section of the Novel Circulating Fluidized Bed System

Riser Height (m)	k_{reaction} (s^{-1})	K (s^{-1})	$k_{\text{mass transfer}}\, a_v$ (s^{-1})	$k_{\text{mass transfer}}$ (m/s)	Sherwood number (–)
3.5	1.95	1.95	Reaction controlled	Reaction controlled	Reaction controlled
7.5	1.95	1.87	46.57	0.0016	0.0119
11.5	1.95	1.32	4.10	0.0001	0.0010
Averaged	1.95	1.71	4.10*	0.0001*	0.0010*

*The averaged values are computed from the upper section constant values.

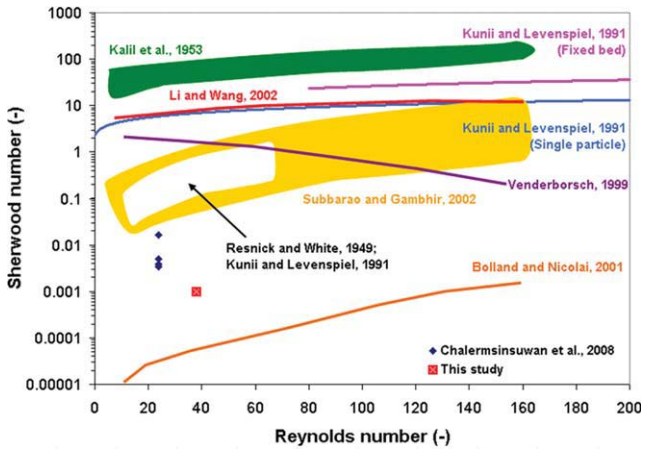

Figure 16. Effect of Reynolds number on Sherwood numbers.

[Color figure can be viewed in the online issue, which is available at wileyonlinelibrary.com.]

are close to each other, implies that the mass transfer has an insignificant role in the reaction. The mass transfer coefficient and Sherwood number, therefore, reflect maldistribution of the hydrodynamics in the system, not the diffusion between the bulk and the surface concentration. To improve the mass transfer, the hydrodynamics behavior inside the system needs to be changed. The effect of Reynolds number on experimental and computed Sherwood numbers is displayed in Figure 16. In this study, the computed Sherwood numbers fall in the experimental range as reviewed by Chalermsinsuwan et al.[41] They are lower than the experimental Sherwood numbers based on the particle diameter for large particles in fluidized and fixed bed systems. The low Sherwood numbers are not a practical concern. They are low in view of the definition of the Sherwood number based on the small particle diameter. For them to be of the order of one, the Sherwood number should be instead defined based on the particle cluster or bubble diameter.

Chemical reaction behavior

Effect of Hydrodynamics Behavior on Reaction Characteristic. Figure 17a displays the contour of CO_2 concentration at 7 s in the novel CFB system. The result shows the bypassing behavior. The CO_2 concentration at the left wall in the bottom region is higher than at the right wall since the CO_2 sorption reaction rate depends on both the CO_2 concentration and the K_2CO_3 solid sorbent volume fraction. The dilution of K_2CO_3 solid sorbent volume fraction at the left wall causes the slow decrease of CO_2 concentration. Conversely, the CO_2 concentration decreases drastically at the right wall of the riser. The time- and area-averaged CO_2 concentration profile in the riser section of the novel CFB system is depicted in Figure 17b. Unlike in the simulation for SO_2 sorption by Therdthianwong and Gidaspow,[8] here, the CO_2 concentration at the top of the riser section is still high, while the SO_2 was almost completely absorbed. The reason for this situation is because of the difference in composition of flue gases. The CO_2 concentration in the flue gases is much higher than the SO_2 concentration. The time- and area-averaged of CO_2 concentration and CO_2 removal percentage at the top of the riser for this novel system are 1.88×10^{-3} kmol/m^3 and 69.16%, respectively. This CO_2 removal percentage is comparable with the industrial scale

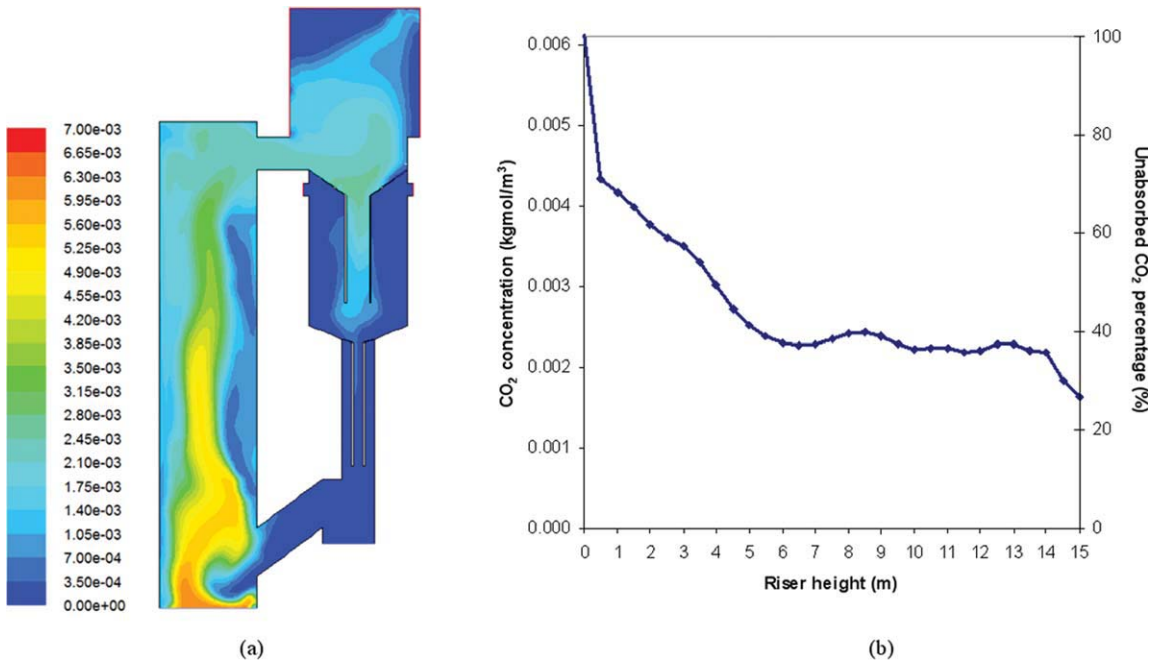

Figure 17. (a) Contour of CO_2 concentration at 7 s and (b) time- and area-averaged CO_2 concentration profile in the riser section of the novel circulating fluidized bed system with v_g = 3 m/s and $k_{reaction}$ = 1.95 s^{-1}.

[Color figure can be viewed in the online issue, which is available at wileyonlinelibrary.com.]

Table 6. Effect of Operating Parameters on the Time- and Area-Averaged CO_2 Concentration and the CO_2 Removal Percentage at the Top of the Riser

Operating Parameter	CO_2 Weight on the Solid Sorbent (kg)	CO_2 Weight on the Flue Gas (kg)	CO_2 Concentration (kmol/m^3)	CO_2 Removal Percentage (%)
Base case				
h = 15.0 m, ρ_s = 1,530 kg/m^3, d_p = 210 μm, v_g = 3 m/s and $k_{reaction}$ = 1.95 s^{-1}	19.68	8.78	1.88×10^{-3}	69.16
Effect of reactor length (h)				
h = 12.5 m	19.56	8.90	1.91×10^{-3}	68.71
h = 17.5 m	20.09	8.37	1.79×10^{-3}	70.58
Effect of solid sorbent density (ρ_s)				
ρ_s = 1730 kg/m^3	19.73	8.73	1.87×10^{-3}	69.31
ρ_s = 1930 kg/m^3	20.11	8.35	1.79×10^{-3}	70.64
Effect of solid sorbent diameter (d_p)				
d_p = 75 μm	17.10	11.36	2.43×10^{-3}	60.09
d_p = 520 μm	19.91	8.55	1.83×10^{-3}	69.95
Effect of inlet gas velocity (v_g)				
v_g = 1 m/s	28.41	0.05	1.24×10^{-5}	99.80
v_g = 5 m/s	13.05	15.41	3.30×10^{-3}	45.85
Effect of reaction rate constant ($k_{reaction}$)				
$k_{reaction}$ = 19.50 s^{-1}	28.45	0.01	1.04×10^{-6}	99.98
$k_{reaction}$ = 195.00 s^{-1}	28.46	0.00	1.72×10^{-26}	100.00

amine or monoethanolamine (MEA) scrubbing method. The reported CO_2 removal is ~70%.[42]

To obtain higher CO_2 removal percentage, the effect of various operating parameters had been explored. In this study, five operating parameters were considered, which were reactor length, solid sorbent density, solid sorbent diameter, inlet gas velocity, and reaction rate constant. When each of the operating parameters was varied, the other operating parameters were then kept at the base case operating condition used in Figure 17. The varied operating parameters were 12.5 and 17.5 m for reactor length, 1730 and 1930 kg/m^3 for solid sorbent density, 75 and 520 μm for solid sorbent diameter, 1 and 5 m/s for inlet gas velocity and 19.50 and 195.00 s^{-1} for reaction rate constant. These ranges of operating parameters were selected from the related experiment. Table 6 summarizes the effect of operating parameters on the time- and area-averaged CO_2 concentration and the CO_2 removal percentage at the top of the riser. Also, the base case operating condition results are shown. From the table, the reactor length, solid sorbent density, solid sorbent diameter, and reaction rate constant have direct proportional with the CO_2 removal; while inlet gas velocity has reverse proportional with the CO_2 removal. However, the reactor length, solid sorbent density, and solid sorbent diameter have less effect on the CO_2 removal than the inlet gas velocity and reaction rate constant. The sorption reaction can be used to explain the reason why each of the operating parameters has the effect on the CO_2 removal. An increase of the CO_2 concentration, the volume fraction of K_2CO_3 solid sorbent and the reaction rate constant provides higher chemical reaction rate inside the system. Then, the explanations are thoroughly discussed for the two operating parameters that have more effect on the CO_2 removal.

The first operating parameter is inlet gas velocity. The changing of inlet gas velocity can alter the system hydrodynamics or the solid volume fraction inside the system.[43] Figures 18a, b demonstrate the contour of CO_2 concentration at 7 s and time- and area-averaged CO_2 concentration profile in the riser section of the novel system with v_g = 1 m/s and $k_{reaction}$ = 1.95 s^{-1}, respectively. Figures 19a, b show the contour of CO_2 concentration at 7 s and time- and area-averaged CO_2 concentration profile in the riser section of the novel system with v_g = 5 m/s and $k_{reaction}$ = 1.95 s^{-1}, respectively. The time- and area-averaged CO_2 concentration profile results confirm that the CO_2 removal depends on the inlet gas velocity. The best and worst CO_2 removals are obtained from the inlet gas velocity of 1 and 5 m/s operating conditions, respectively. The contour of CO_2 concentration results confirm the bypassing behavior as observed in Figure 17. Table 7 displays the effect of inlet gas velocities on the axial and radial dispersion coefficients in the riser section of the novel system. The gas and solid axial dispersion coefficients increase with the inlet gas velocity, while the gas and solid radial dispersion coefficients have no trend. The effect of inlet gas velocities on the mass transfer coefficients and the Sherwood numbers in the riser section of the novel system is summarized in Table 8. They slightly increase with the inlet gas velocity. In view of the change in the order of magnitudes, these system parameters have little effect on CO_2 removal. Considering the system parameters, the main explanation for the high CO_2 removal, therefore, is the reduction of axial dispersion coefficient, which further gives more time for gas and solid to react in the system. However, the reason for the high CO_2 removal with the inlet gas velocity of 1 m/s also can be explained using the solid volume fraction distribution as already proposed. With this operating condition, the system is extremely dense corresponding to the new observed flow regime called circulating-turbulent fluidized bed.[43]

The second parameter that can be changed is the reaction rate constant. This can be done by the improvement of the current K_2CO_3 sorbent properties. As shown in the chemical

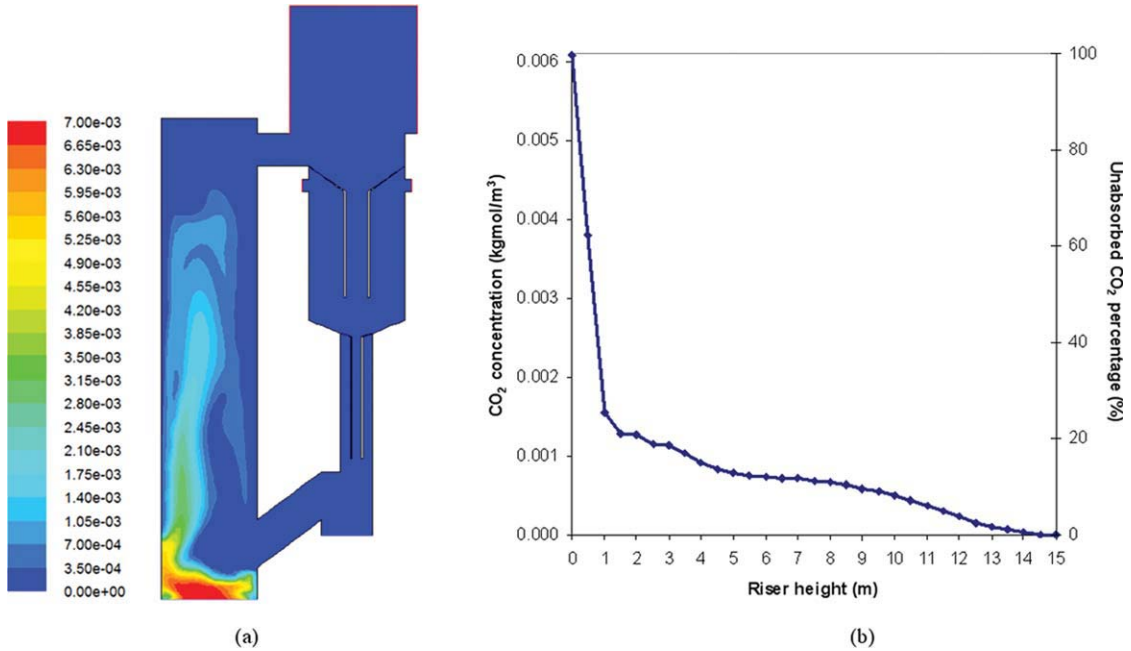

Figure 18. (a) Contour of CO_2 concentration at 7 s and (b) time- and area-averaged CO_2 concentration profile in the riser section of the novel circulating fluidized bed system with v_g = 1 m/s and $k_{reaction}$ = 1.95 s^{-1}.

[Color figure can be viewed in the online issue, which is available at wileyonlinelibrary.com.]

reaction model part, there are attempts to develop better K_2CO_3 solid sorbents with a high absorption performance. Here, we assume such a solid sorbent is already developed. Hence, we simulated the system with two higher reaction rate constants. Figures 20a, b demonstrate the contour of CO_2 concentration at 7 s and time- and area-averaged CO_2 concentration profile in the riser section of the novel system with v_g = 3 m/s and $k_{reaction}$ = 19.50 s^{-1}, respectively. Figures 21a, b show the contour of CO_2 concentration at 7 s and time- and area-averaged CO_2 concentration profile in the

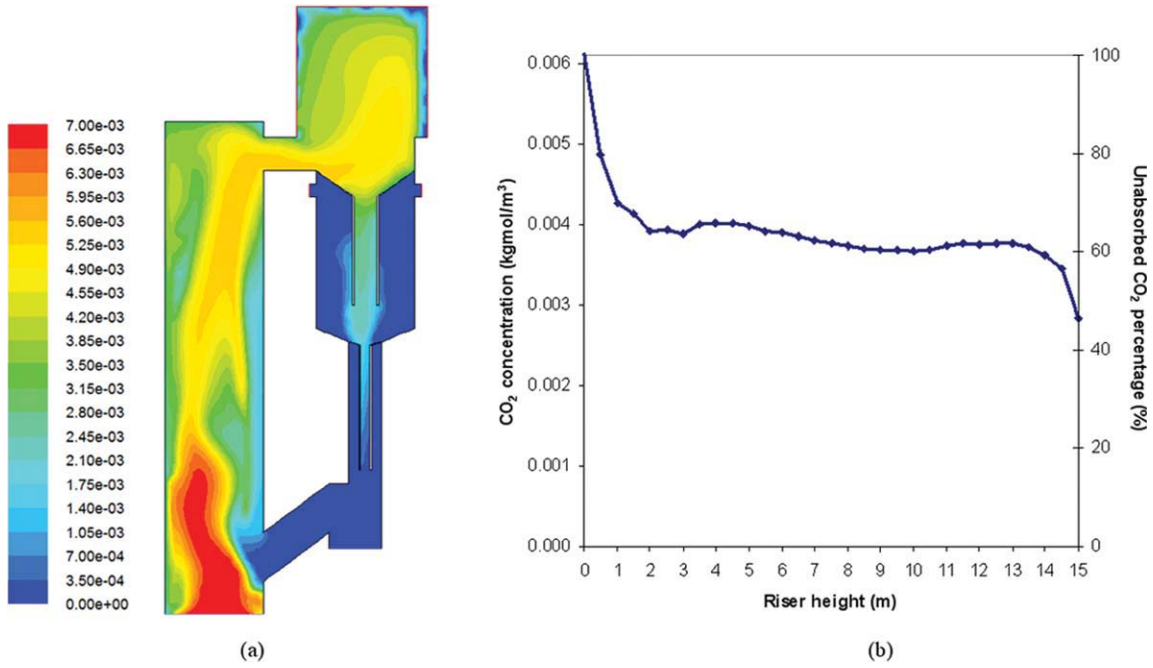

Figure 19. (a) Contour of CO_2 concentration at 7 s and (b) time- and area-averaged CO_2 concentration profile in the riser section of the novel circulating fluidized bed system with v_g = 5 m/s and $k_{reaction}$ = 1.95 s^{-1}.

[Color figure can be viewed in the online issue, which is available at wileyonlinelibrary.com.]

Table 7. Effect of Inlet Gas Velocities on the Axial and Radial Dispersion Coefficients in the Riser Section of the Novel System with $k_{reaction} = 1.95\ s^{-1}$

Inlet Gas Velocity (m/s)	Solid Dispersion Coefficients (m^2/s)		Gas Dispersion Coefficients (m^2/s)	
	Axial	Radial	Axial	Radial
1	0.0670	0.0143	0.0682	0.0179
3	0.4309	0.0879	0.4663	0.0897
5	0.8852	0.0401	0.9693	0.0420

riser section of the novel system with $v_g = 3$ m/s and $k_{reaction} = 195.00\ s^{-1}$, respectively. These results confirm that CO_2 removal will improve if solids sorbents can be prepared to have much higher reaction rates, which is consistent with the reaction rate Eq. 21. In addition, the reason for the high CO_2 removal can be explained using the system parameters. Table 9 summarizes the effect of reaction rate constants on the axial and radial dispersion coefficients in the riser section of the novel system. From the computations, there is no clear trend of the gas and solid axial dispersion coefficients, while there is a trend of the gas and solid radial dispersion coefficients. The radial dispersion coefficient increases with the reaction rate constant. Table 10 illustrates the effect of reaction rate constants on the mass transfer coefficients and the Sherwood numbers in the riser section of the novel system. The mass transfer coefficients and the Sherwood numbers also increase with the reaction rate constant. Both the increase of radial dispersion and mass transfer coefficients can improve system mixing and give a higher CO_2 removal.

Effect of Temperature Rise. To determine the effect of temperature rise on the removal efficiency, the reaction rate constant was expressed using Onischak and Gidaspow[15] experimental data as a function of gas temperature as follows:

$$k_{reaction} = 0.55\ \exp(-(-3609)/RT_g), \tag{31}$$

where R is the gas constant and T_g is the temperature of gas phase. The rate of reaction is then obtained by substituting Eq. 31 into Eq. 21.

The energy equations for the gas and solids in the FLUENT were also used for this nonisothermal simulation with an adiabatic wall condition.

For gas phase:

$$\frac{\partial}{\partial t}\left(\varepsilon_g \rho_g H_g\right) + \nabla \cdot \left(\varepsilon_g \rho_g v_g H_g\right) = -\varepsilon_g \frac{\partial P}{\partial t} + \tau_g : \nabla \cdot v_g + S_g + Q_{sg}, \tag{6}$$

For solid phase:

$$\frac{\partial}{\partial t}\left(\varepsilon_s \rho_s H_s\right) + \nabla \cdot \left(\varepsilon_s \rho_s v_s H_s\right) = -\varepsilon_s \frac{\partial p_s}{\partial t} + \tau_s : \nabla \cdot v_s + S_s + Q_{gs}, \tag{7}$$

with $H_g = \int c_{p,g} dT_g$ and $H_s = \int c_{p,s} dT_s$

Figure 22a displays the axial time- and area-averaged gas and solid temperature profiles in the riser section with $v_g = 3$ m/s and $k_{reaction} = 0.55\ \exp(3609/RT)\ s^{-1}$. At the inlet, the gas temperature is 343.15 K which is the flue gas temperature used in this study. The temperature peaks at the bottom section are due to the heat of chemical reaction. Then, the temperatures slightly increase along the riser through the outlet. At the top of the riser or the section beyond the outlet, the temperatures decrease. The reason may be because of the absence of CO_2 and solid sorbent in this area. Thus, the sorption reaction has not occurred. The radial time-averaged gas temperature profiles in the riser section with $v_g = 3$ m/s and $k_{reaction} = 0.55\ \exp(3609/RT)\ s^{-1}$ at three different riser heights are illustrated in Figure 22b. These three different heights are also at 3.5, 7.5, and 11.5 m, similar to those in previous parts. Asymmetric profiles are obtained, which are consistent with the sorption reaction inside the system. Table 11 shows that the relatively small temperature rise computed with the code is correct. For the experimentally determined rate of reaction in Figure 22, the temperature rise in the CFB riser section was only about 10 K. In Table 11, the same small temperature rise is obtained from an overall time-averaged energy balance. The reason for the small temperature rise is due to the large recirculation rates. Table 3 summarizes the recirculation rate to be 635 kg/m^2 s at the inlet gas velocity of 3 m/s. CFB combustors, such as the PYROFLOW system reviewed by Gidaspow,[17] operate at such high fluxes. Hence, in this system, the sorber does not require external cooling. In a bubbling fluidized bed Na_2CO_3 sorber being designed by the US, DOE and Research Triangle Institute (RTI) cooling tubes are put into the bed to remove the heat.[44]

Table 8. Effect of Inlet Gas Velocities on the Mass Transfer Coefficients and Sherwood Numbers in the Riser Section of the Novel System with $k_{reaction} = 1.95\ s^{-1}$

Inlet Gas Velocity (m/s)	Riser Height (m)	$k_{mass\ transfer}\ a_v$ (s^{-1})	$k_{mass\ transfer}$ (m/s)	Sherwood Number (–)
1	3.5	5.09	0.00018	0.0013
	7.5	1.25	0.00004	0.0003
	11.5	0.94	0.00003	0.0002
	Averaged	2.43	0.0001	0.0006
3	3.5	Reaction controlled	Reaction controlled	Reaction controlled
	7.5	46.57	0.0016	0.0119
	11.5	4.10	0.0001	0.0010
	Averaged	4.10*	0.0001*	0.0010*
5	3.5	Reaction controlled	Reaction controlled	Reaction controlled
	7.5	Reaction controlled	Reaction controlled	Reaction controlled
	11.5	Reaction controlled	Reaction controlled	Reaction controlled
	Averaged	Reaction controlled	Reaction controlled	Reaction controlled

*The averaged values are computed from the upper section constant values.

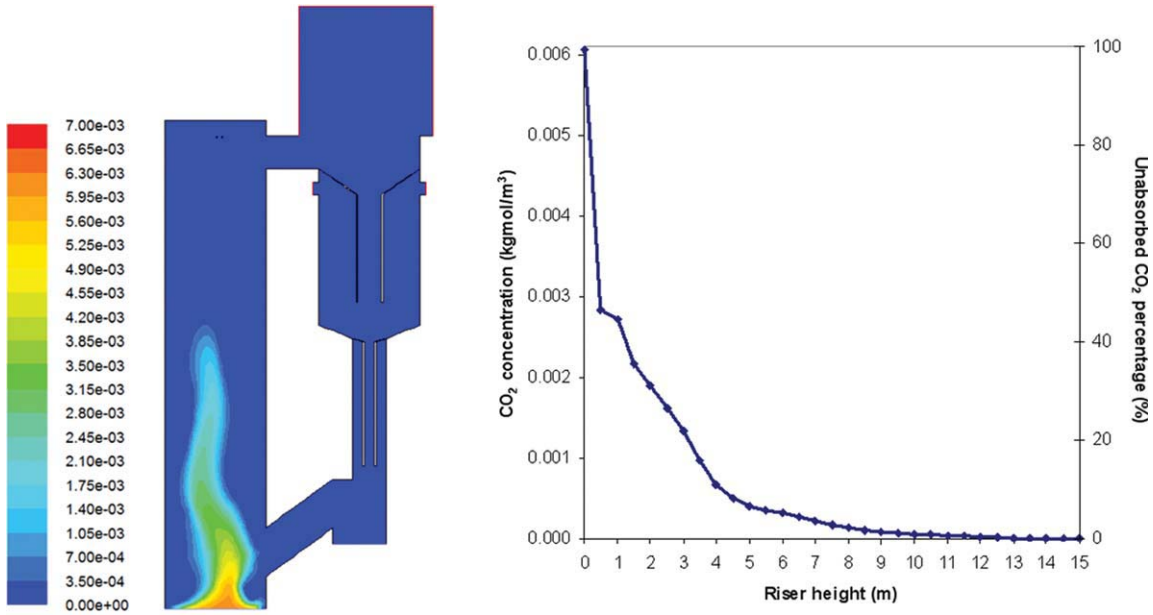

Figure 20. (a) Contour of CO_2 concentration at 7 s and (b) time- and area-averaged CO_2 concentration profile in the riser section of the novel circulating fluidized bed system with v_g = 3 m/s and $k_{reaction}$ = 19.50 s^{-1}.

[Color figure can be viewed in the online issue, which is available at wileyonlinelibrary.com.]

Figures 23a, b show the contour of CO_2 concentration at 7 s and time- and area-averaged CO_2 concentration profile in the riser section with $v_g = 3$ m/s and $k_{reaction} = 0.55 \exp(3609/RT)$ s^{-1}. For this operating condition, the time- and area-averaged of CO_2 concentration is 2.04×10^{-3} kmol/m^3 and CO_2 removal percentage is 66.48% at the top of the riser. The results are consistent with the result in Figure 17 but the CO_2 concentration is slightly lower, which confirms the statement from

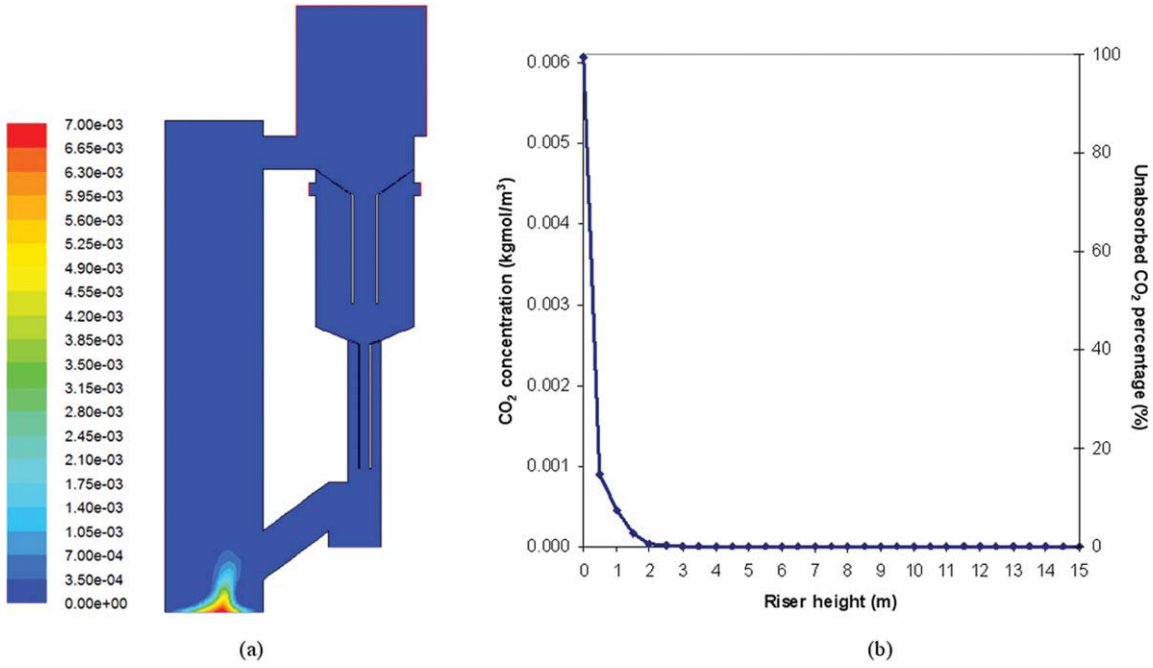

Figure 21. (a) Contour of CO_2 concentration at 7 s and (b) time- and area-averaged CO_2 concentration profile in the riser section of the novel circulating fluidized bed system with v_g = 3 m/s and $k_{reaction}$ = 195.00 s^{-1}.

[Color figure can be viewed in the online issue, which is available at wileyonlinelibrary.com.]

Table 9. Effect of Reaction Rate Constants on the Axial and Radial Dispersion Coefficients in the Riser Section of the Novel System with v_g = 3 m/s

Reaction Rate Constant (s^{-1})	Solid Dispersion Coefficients (m^2/s)		Gas Dispersion Coefficients (m^2/s)	
	Axial	Radial	Axial	Radial
1.95	0.4309	0.0879	0.4663	0.0897
19.50	0.5885	0.1578	0.6343	0.1909
195.00	0.5290	0.2169	0.5361	0.2171

the literature that the reaction rate for CO_2 capture decreases with the increasing of temperature. Comparing with the base case condition, the percentage difference is only 3.88%, which verifies the validity of the results from the fixed reaction rate constant. The proposed K_2CO_3 solid sorbent based sorption-regeneration CFB system is thus a promising alternative for the capture of CO_2 from the flue gases.

Computed Low Gas-Particle Nusselt Number. Similar to the mass transfer coefficient and the Sherwood number, the heat transfer coefficient (h_c) and the Nusselt number can also be calculated from this simulation. These two system parameters explain the heat transfer phenomena inside the riser system. With the same methodology for calculation of the mass transfer coefficient and the Sherwood number, the heat transfer coefficient (h_c) and the Nusselt number (Nu) can be obtained from the temperature data. Integration of conservation of energy equation over time and over the riser diameter for gas phase gives the one dimensional steady state balance. Solving the equation gives:

$$\ln(T_s - T_g) = \ln(T_s - T_{g,0}) - \frac{h_c}{\varepsilon_g \rho_g v_y c_{pg}} Y \qquad (32)$$

where T_s is the temperature of solid phase, c_{pg} is the heat capacity at constant pressure of gas phase and the subscript "0" is the initial temperature of gas phase. The linear plot of natural logarithm of the temperature difference between the phase vs. the height of the riser gives the slope, which finally gives the heat transfer coefficient. The Nusselt number is then computed by Eq. 33 below:

$$Nu = \frac{h_c d_p}{k} \qquad (33)$$

where k is thermal conductivity.

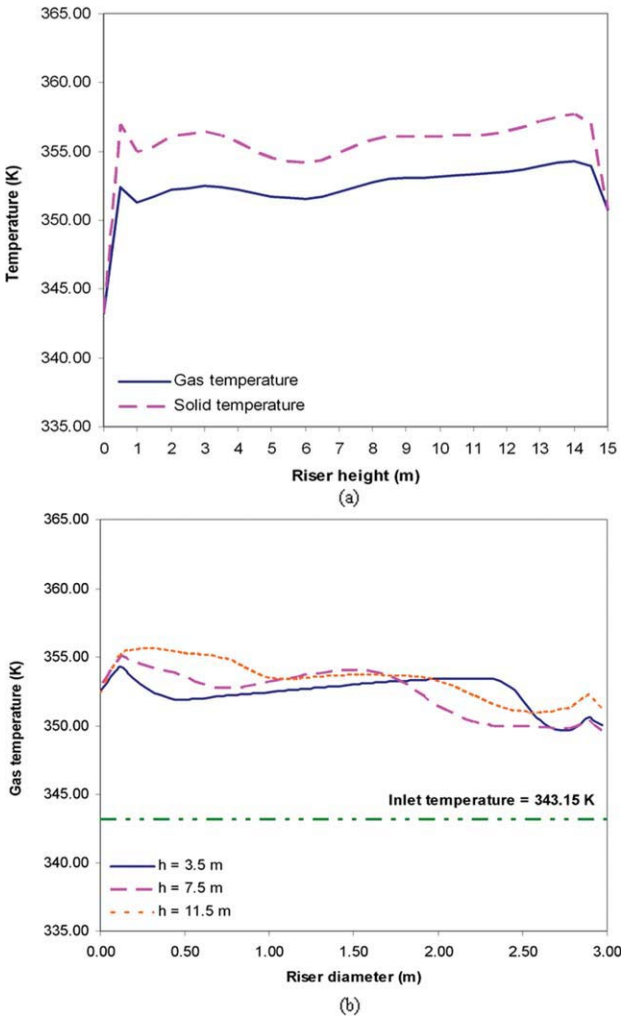

Figure 22. (a) Axial time- and area-averaged gas and solid temperature profiles and (b) radial time-averaged gas temperature profiles in the riser section of the novel system with v_g = 3 m/s and $k_{reaction}$ = 0.55exp(3609/RT) s^{-1}.

Note: Most of the temperature rise occurs in the first meter of the scrubber consistent with CO_2 drop in Figure 23b. [Color figure can be viewed in the online issue, which is available at wileyonlinelibrary.com.]

Table 10. Effect of Reaction Rate Constants on the Mass Transfer Coefficients and Sherwood Numbers in the Riser Section of the Novel System with v_g = 3 m/s

Reaction Rate Constant (s^{-1})	Riser Height (m)	$k_{mass\ transfer}\ a_v$ (s^{-1})	$k_{mass\ transfer}$ (m/s)	Sherwood Number (–)
1.95	3.5	Reaction controlled	Reaction controlled	Reaction controlled
	7.5	46.57	0.0016	0.0119
	11.5	4.10	0.0001	0.0010
	Averaged	4.10*	0.0001*	0.0010*
19.50	3.5	10.27	0.0004	0.0026
	7.5	5.90	0.0002	0.0015
	11.5	6.16	0.0002	0.0016
	Averaged	7.44	0.0003	0.0019
195.00	3.5	27.47	0.0010	0.0070
	7.5	26.32	0.0009	0.0067
	11.5	35.00	0.0012	0.0089
	Averaged	29.60	0.0010	0.0076

*The averaged values are computed from the upper section constant values.

Table 11. A Check on Temperature Rise in the Riser Section of the Novel System

Reaction Rate Constant (s^{-1})	Energy Flow at the Riser Inlet (MJ/s)	Energy Flow at the Riser Outlet (MJ/s)	Released Heat in the Riser Section	
			From Energy Flows (MJ/s)	From Sorption Reaction (MJ/s)
$0.55 \exp(-(-3609)/RT_g)$	54.705	59.931	5.226	5.222

The time-averaged energy balance in the riser section:

Rate of energy flow = Energy flow at the riser outlet − Energy flow at the riser inlet
= Released heat in the riser section (due to sorption reaction)
= Averaged sorption reaction rate × Heat of sorption reaction

Example.
For reaction rate constant ($k_{reaction}$) = 0.55 exp(−(−3609)/RT_g) s^{-1}:

Rate of energy flow = Energy flow at the riser outlet − Energy flow at the riser inlet
= 59.931(MJ/s) − 54.705(MJ/s)
= 5.226(MJ/s)

Rate of energy flow = Averaged sorption reaction rate × Heat of sorption reaction
= 0.036(kgmol/s) × (−145.067)(MJ/kgmol)
= −5.222(MJ/s)(Minus sign = Exothermic reaction)

Rate of energy flow = 5.226 (MJ/s) ≈ 5.222 (MJ/s)
Estimated system temperature rise from the time-averaged energy balance = 9.741 K
Therefore, the energy in the riser section of the novel system is balanced and the estimated system temperature rise is consistent with the simulated result (≈10 K). The numerical difference is possibly because of the time-averaged round off error.

The computed heat transfer coefficient and Nusselt number for this system with v_g = 3 m/s and $k_{reaction}$ = 0.55 exp(3609/RT) s^{-1} are 0.0075 J/s m K and 0.0001, respectively. The computed Nusselt number falls in the experimental range as reviewed by Kunii and Levenspiel.[45] It is also lower than the experimental Nusselt numbers based on the particle diameter for large particles in fluidized and fixed bed systems, similar to the Sherwood number in mass transfer.

Conclusions

(1) A kinetic theory based hydrodynamic model with experimentally determined sorption rates for reaction between CO_2 and pellets of solid supported K_2CO_3 is used to design a compact CFB for removal of CO_2 from flue gases. This unit is similar to the CFB coal combustor operating with calcined limestone for sulfur removal. It can handle large volumetric flow rates with a reasonable pressure drop. For a high system

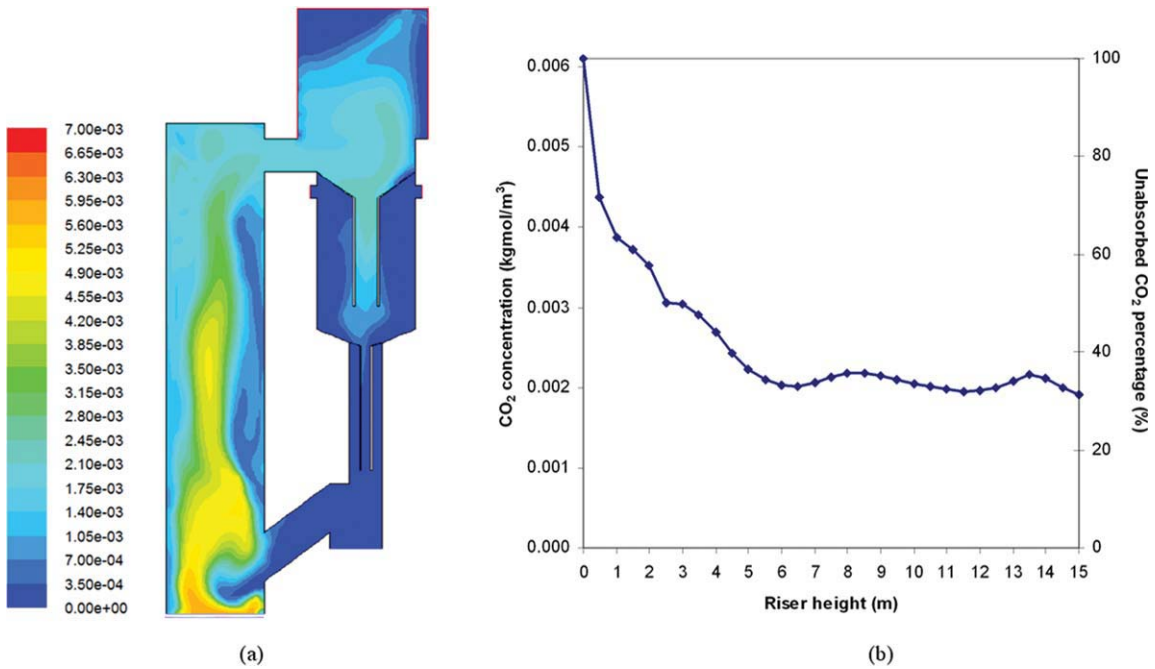

Figure 23. (a) Contour of CO_2 concentration at 7 s and (b) time- and area-averaged CO_2 concentration profile in the riser section of the novel circulating fluidized bed system with v_g = 3 m/s and $k_{reaction}$ = 0.55exp(3,609/RT) s^{-1}.

[Color figure can be viewed in the online issue, which is available at wileyonlinelibrary.com.]

performance, the low temperature heat evolved during sorption can be upgraded using a heat pump concept.

(2) Conventional fluidized bed design uses empirical dispersion and mass transfer coefficients. In the multiphase kinetic theory approach presented here these coefficients are computed. The axial, solid and gas, dispersion, and mass transfer coefficients are in the range of reported measurements while the radial, solid and gas, dispersion coefficients are higher than the reported values for smaller bed diameters. This good mixing counteracts the operation of the riser in the core-annular regime and produces a compact unit. The low computed Sherwood number does not imply a large mass transfer resistance in the fluid, since the overall reaction resistance and the input reaction rate constant are close to each other. The resistance is due to reaction and diffusion in the pellet.

(3) With the sorbent prepared using published information, ~70% of the CO_2 is removed form the flue gases. To obtain higher CO_2 removal percentage, the effect of various operating parameters is explored. The reactor length, solid sorbent density and solid sorbent diameter have less effect on the CO_2 removal than the inlet gas velocity and reaction rate constant in this study ranges. By increasing the reaction rate constant, complete CO_2 removal can be achieved in this system. A high CO_2 removal can also be achieved by lowering the gas velocity. But then the sorbent volume will rise for a given flue gas load.

(4) To determine the effect of temperature rise on the removal efficiency of CO_2, the reaction rate constant was expressed as a function of temperature and a simulation was repeated with the energy equations for the gas and solids. The average gas temperature rise of about 10 K did not significantly decrease the percent removal of CO_2 in this CFB system. This simulation shows that we do not need internal or external cooling in our sorber.

Acknowledgments

The authors gratefully acknowledge financial support of this study by the Thailand Research Fund through the Royal Golden Jubilee Ph.D. Program (Grant No. PHD/0021/2550). This study also was partially supported by the Center for Petroleum, Petrochemicals, and Advanced Materials.

Notation

a_v = external surface per volume of catalyst (m^{-1})
c_p = heat capacity at constant pressure (J/kg K)
C = concentration (kgmol/m^3)
C_{D0} = drag coefficient (–)
d_p = particle diameter (m)
D = diameter of riser (m)
D = molecular diffusivity (m^2/s)
D_i = dispersion coefficient (m^2/s)
e = restitution coefficient between particles (–)
e_W = restitution coefficient between particle and wall (–)
g = gravity force (m/s^2)
g_0 = radial distribution function (–)
G_s = solid sorbent circulation rate (kg/m^2 s)
h = height of riser (m)
h_c = heat transfer coefficient (J/s m K)
H = specific enthalpy (J/kg)
ΔH = heat of reaction (J/kgmol)
I = unit tensor (–)
k = thermal conductivity (J/s m K)
$k_{mass\ transfer}$ = mass transfer coefficient (m/s)
$k_{reaction}$ = reaction rate constant (s^{-1})
K = overall resistance (m/s)
$\dot{m}$ = system molar flow rate (kgmol/s)
M = metal of an alkaline (–)
n = unit vector (–)
Nu = Nusselt number (–)
p_s = solid pressure (Pa)
P = gas pressure (Pa)
$\dot{Q}$ = heat flow (J/s)
Q_{gs} = intensity of heat exchange from gas phase to solid phase (J/s m^3)
Q_{sg} = intensity of heat exchange from solid phase to gas phase (J/s m^3)
r = reaction rate (kgmol/s m^3)
R = gas constant (kJ/kmol K)
R_j = reaction rate of specie "j" (kg/s m^3)
Re_k = Reynolds number (–)
S = source term (e.g., due to chemical reaction) (J/s m^3)
Sh = Sherwood number (–)
t = time (s)
T = temperature (K)
T_L = Lagrangian integral time scale (s)
v = velocity (m/s)
v' = velocity fluctuation (m/s)
$v_{s,slip}$ = slip velocity of particle at the wall (m/s)
$v_{st,W}$ = tangential velocity of particle at the wall (m/s)
y_j = mass fraction of each species (–)
Y = axial or vertical distance (m)

Greek letters

β_{gs} = gas–solid interphase drag coefficient (kg/s m^3)
ε = volume fraction (–)
$\varepsilon_{s,max}$ = solid volume fraction at maximum packing (–)
ϕ = specularity coefficient (–)
γ_s = collisional dissipation of solid fluctuating energy (kg/m s^3)
γ_W = collisional dissipation of solid fluctuating energy at the wall (kg/m s^3)
κ_s = conductivity of the fluctuating energy (kg/m s)
μ = viscosity (kg/m s)
π = mathematical constant ≈ 3.14 (–)
ρ = density (kg/m^3)
θ = granular temperature (m^2/s^2)
θ_t = turbulent granular temperature (m^2/s^2)
θ_W = granular temperature at the wall (m^2/s^2)
τ = stress tensor (Pa)
ξ_s = bulk viscosity (kg/m s)

Subscripts

C = cold region
CO_2 = carbon dioxide specie
g = gas phase
H = hot region
i = i direction
j = j specie
R = regeneration reaction
s = solid phase
S = sorption reaction
x = radial direction
y = axial direction
z = radial direction
0 = initial condition

Literature Cited

1. Pennline HW, Luebke DR, Jones KL, Myers CR, Morsi BI, Heintz YJ, Ilconich JB. Progress in carbon dioxide capture and separation research for gasification-based power generation point sources. *Fuel Process Technol.* 2008;89:897–907.
2. Konduru N, Lindner P, Assaf-Anid NM. Curbing the greenhouse effect by carbon dioxide adsorption with zeolite 13X. *AIChE J.* 2007;53:3137–3143.
3. Zhen-shan L, Ning-sheng C, Croiset E. Process analysis of CO_2 capture from flue gas using carbonation/calcination cycles. *AIChE J.* 2008;54:1912–1925.

4. Zhang J, Singh R, Webley PA. Alkali and alkaline-earth cation exchanged chabazite zeolites for adsorption based CO_2 capture. *Microporous Mesoporous Mater*. 2008;111:478–487.
5. Gunther M. *Carbon finance comes of age*. In: Moore AS, editor. *Fortune*, *Vol*. 157. US: Fortune, Inc., 2008:124–132.
6. Metz B, Davidson O, de Coninck H, Loos M, Meyer L. *Carbon Dioxide Capture and Storage*, 1st ed. Cambridge, UK: Cambridge University Press, 2005.
7. Chakma A. Formulated solvents: new opportunities for energy efficient separation of acid gases. *Energy Sources*. 1999;21:51–62.
8. Therdthianwong A, Gidaspow D. Hydrodynamics and SO_2 sorption in a CFB loop. Presented at the 4th International Conference on Circulating Fluidized Bed, Pittsburgh, US, 1993.
9. Smith JM, Van Ness HC, Abbott MM. *Introduction to Chemical Engineering Thermodynamics*, 5th ed. Singapore: McGraw-Hill Companies, 1996.
10. King CJ. *Separation Processes* 2nd ed. New York, US: McGraw-Hill Companies, 1980.
11. Gupta H, Fan LS. Carbonation-calcination cycle using high reactivity calcium oxide for carbon dioxide separation from flue gas. *Ind Eng Chem Res*. 2002;41:4035–4042.
12. Lee SC, Kim JC. Dry potassium-based sorbents for CO_2 capture. *Catal Surv Asia*. 2007;11:171–185.
13. Weimer T, Berger R, Hawthorne C, Abanades JC. Lime enhanced gasification of solid fuels: examination of a process for simultaneous hydrogen production and CO_2 capture. *Fuel*. 2008;87:1678–1686.
14. Gidaspow D. *Separation of gaseous mixtures by regenerative sorption on porous solids. I. A fluid porous solid reaction model with structural changes*. In: Li NN, editor. *Recent Development in Separation Science*, *vol*. 2. Baco Raton, FL: CRC Press, 1972:59–70.
15. Onischak M, Gidaspow D. Kinetics of the reaction of CO_2 with solid K_2CO_3. Presented at the 73rd National AIChE Meeting, Minneapolis, US, 1972.
16. Hayashi H, Taniuchi J, Furuyashiki N, Sugiyama S, Hirano S, Shigemoto N, Nonaka T. Efficient recovery of carbon dioxide from flue gases of coal-fired power plants by cyclic fixed-bed operations over K_2CO_3-on-carbon. *Ind Eng Chem Res*. 1998;37:185–191.
17. Gidaspow D. *Multiphase Flow and Fluidization: Continuum and Kinetic Theory Description*, 1st ed. New York, US: Academic Press, 1994.
18. Ding J, Gidaspow D. A bubbling fluidization model using kinetic theory of granular flow. *AIChE J*. 1990;36:523–538.
19. Tsuo YP, Gidaspow D. Computation of flow patterns in circulating fluidized beds. *AIChE J*. 1990;36:885–896.
20. Chalermsinsuwan B, Kuchonthara P, Piumsomboon P. Effect of circulating fluidized bed reactor riser geometries on chemical reaction rates by using CFD simulations. *Chem Eng Process*. 2009;48:165–177.
21. Onischak M, Gidaspow D. *Separation of gaseous mixtures by regenerative sorption on porous solids. II. Regenerative separation of CO_2*. In: Li NN, editor. *Recent Development in Separation Science*, *vol*. 2. Baco Raton, FL: CRC Press, 1972:71–93.
22. Onischak J, Baker B. Development of a prototype regenerable carbon dioxide absorber for portable life support systems. *J Eng Ind*. 1978;100:383–385.
23. Ghezelayagh H, Gidaspow D. Micro-macropore model for sorption of water on silica gel in a dehumidifier. *Chem Eng Sci*. 1982;37:1181–1197.
24. Hirano S, Shigemoto N, Yamada S, Hayashi H. Cyclic fixed-bed operations over K_2CO_3-on-carbon for the recovery of carbon dioxide under moist conditions. *Bull Chem Soc Jpn*. 1995;68:1030–1035.
25. Okunev AG, Sharonov VE, Aristov YI, Parmon VN. Sorption of carbon dioxide from wet gases by K_2CO_3-in-porous matrix: influence of the matrix nature. *React Kinet Catal Lett*. 2000;71:355–362.
26. Sharonov VE, Tyshchishchin EA, Moroz EM, Okunev AG, Aristov YI. Sorption of CO_2 from humid gases on potassium carbonate supported by porous matrix. *Russ J Appl Chem*. 2001;74:409–413.
27. Sharanov VE, Okunev AG, Aristov YL. Kinetics of carbon dioxide sorption by the composite material K_2CO_3 in Al_2O_3. *React Kinet Catal Lett*. 2004;82:363–369.
28. Park SW, Sung DH, Choi BS, Lee JW, Kumazawa H. Carbonation kinetics of potassium carbonate by carbon dioxide. *J Ind Eng Chem*. 2006;12:522–530.
29. Johnson PC, Jackson R. Frictional-collisional constitutive relations for granular materials, with application to plane shearing. *J Fluid Mech*. 1987;176:67–93.
30. Sinclair JL, Jackson R. Gas-particle flow in a vertical pipe with particle–particle interaction. *AIChE J*. 1989;35:1473–1486.
31. Miller A, Gidaspow D. Dense, vertical gas-solid flow in a pipe. *AIChE J*. 1992;38:1801–1815.
32. Tartan M, Gidaspow D. Measurement of granular temperature and stresses in risers. *AIChE J*. 2004;50:1760–1775.
33. Brereton CMH, Grace JR. End effects in circulating fluidized bed hydrodynamics. Presented at the 4th International Conference on Circulating Fluidized Bed, Pittsburgh, US, 1993.
34. Qia-yu Z, Hai Z. Experimental study of the effect of bed exits with different geometric structure on internal recycling of bed material in CFB boilers. Presented at the 4th International Conference on Circulating Fluidized Bed, Pittsburgh. US, 1993.
35. Grace JR, Avidan AA, Knowlton TM. *Circulating Fluidized Beds* 1st ed. London, UK: Blackie Academic & Professional, 1997.
36. Lehner P, Wirth KE. Characterization of the flow pattern in a downer reactor. *Chem Eng Sci*. 1999;54:5471–5483.
37. Chalermsinsuwan B, Piumsomboon P, Gidaspow D. Kinetic theory based computation of PSRI riser. I. Estimate of mass transfer coefficient. *Chem Eng Sci*. 2009;64:1195–1211.
38. Kashyap M, Gidaspow D, Driscoll M. Effect of electric field on the hydrodynamics of fluidized nanoparticles. *Powder Technol*. 2008;183:441–453.
39. Gidaspow D, Huilin L. Collisional viscosity of FCC particles in a CFB. *AIChE J*. 1996;42:2503–2510.
40. Jiradilok V, Gidaspow D, Damronglerd S, Koves WJ, Mostofi R. Kinetic theory based CFD simulation of turbulent fluidization of FCC particles in a riser. *Chem Eng Sci*. 2006;61:5544–5559.
41. Chalermsinsuwan B, Piumsomboon P, Gidaspow D. Kinetic theory based computation of PSRI riser. II. Computation of mass transfer coefficient with chemical reaction. *Chem Eng Sci*. 2009;64:1212–1222.
42. Rochelle GT. *Amine scrubbing for CO_2 capture*. In: Steven C, editor. *Science*. US: AAAS, 2009;325:1652–1654.
43. Zhu H, Zhu J. Gas-solids flow structures in a novel circulating turbulent fluidized bed. *AIChE J*. 2008;54:1213–1223.
44. Coleman LJI, Turk BS, Gupta RP. Integration of CFD and experimental-based design and development of fluidized-bed-reactor-based processes. Presented at the 2009 AIChE Annual Meeting, Nashville, US, 2009.
45. Kunii D, Levenspiel O. *Fluidization Engineering*, 2nd ed. Boston, MA: Butterworth-Heinemann, 1991.

Manuscript received Feb. 1, 2009, and revision received Jan. 26, 2010.